2. Materials and methods

2.1. Animals

Male C57/BL6J mice weighing 25–30 g (8–14 weeks old) were housed in a temperature (25 ± 2 °C)- and moisture (50%)-controlled room with a 12 h light/dark cycle (6:00 AM/6:00 PM). The mice were fed standard mouse chow (Oriental Yeast, Osaka) and tap water *ad libitium*, and used as wild-type mice.

Generation of GIPR$^{-/-}$ mice and GLP-1 receptor-deficient mice (GLP-1R$^{-/-}$ mice) was described previously [2,6]. GLP-1R$^{-/-}$ mice were kindly provided by Dr. Daniel J. Drucker [6]. Age-matched male GIPR$^{-/-}$ and GLP-1R$^{-/-}$ mice were used in the experiments. The Animal Care Committee of Kyoto University Graduate School of Medicine approved animal care and procedures.

2.2. Materials

Synthetic human GIP was purchased from Peptide Institute (Osaka, Japan). The somatostatin receptor antagonist, cyclo(7-aminoheptanoyl-PHE-D-TRP-LYS-THR(BZL)) (cyclosomatostatin (CSS)) and somatostatin 28 (SST) were from Sigma Chemical Co. (St. Louis, MO). All other chemicals were of reagent grade.

2.3. Perfusion experiment

Single-pass perfusion method [7] was used to measure the effect of exogenous GIP or SST on intestinal glucose absorption using C57/BL6J mice. Preperfusion was done for a 45 min equilibration period and the samples were discarded. Three 15 min samples were then collected. GIP or SST was administered intraperitoneally at 60 min after starting the preperfusion according to the protocol (Fig. 1A). The change of absorption was calculated as the glucose concentration of the first sample collected (Period 1) minus the glucose concentration of the last sample collected (Period 2), and expressed as per centimeter perfused bowel. Negative values indicate an inhibitory effect on absorption; positive values indicate an increased effect on absorption.

2.4. Glucose uptake in jejunum in vitro

Incorporation of D-glucose into everted jejunal rings was determined as described previously [8]. SGLT-dependent glucose uptake for 15 min was determined as the glucose uptake in the absence of phlorizin minus the glucose uptake in the presence of phlorizin.

2.5. Small intestinal transit after intraperitoneal administration of GIP

Transit through the stomach and small intestine was measured by administering a non-absorbed marker containing 10% charcoal suspension in 5% gum Arabic, as previously described [9]. The mice were given 0.2 ml of the suspension by gavage through a straight blunt-ended feeding needle. GIP (50 nmol/kg body weight) or SST (75 nmol/kg body weight) or vehicle (saline) was administered intraperitoneally 15 min prior to the administration of the non-absorbed marker. CSS (1 μg/kg body weight), or vehicle (saline) was intraperitoneally administered 10 min prior to GIP administration.

2.6. Plasma GIP and SST assays

Blood was collected from the tail vein before the intraperitoneal administration of GIP (50 nmol/kg body weight) and collected again 20 min after the administration. ELISA assay kit was used according to the manufacture's instruction for the determination of plasma total GIP concentration (Linco Research, St. Charles, MO) and SST concentration (Phoenix Pharmaceuticals INC., Belmont, CA), respectively.

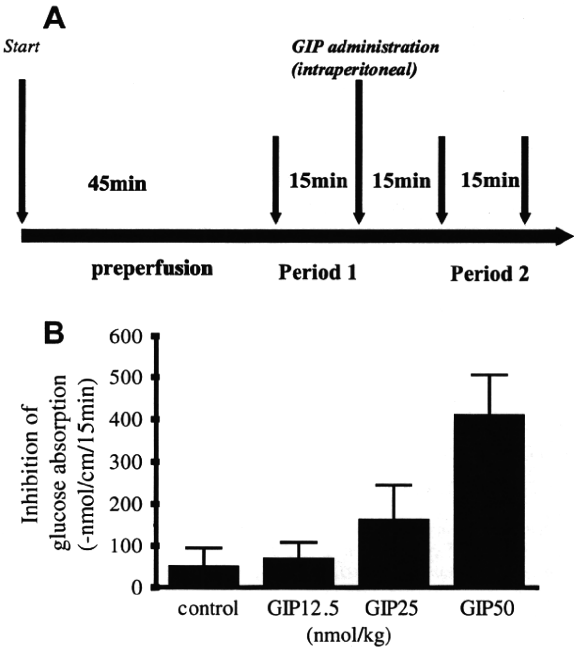

Fig. 1. (A) Diagram showing the sampling protocol of intestinal perfusion. The flow rate of the perfusion fluid was 2 ml/15 min. Perfusion began with an equilibration period of 45 min, which samples were discarded. The samples of Period 1 and Period 2 were then collected. GIP was administered intraperitoneally 60 min after the beginning of preperfusion. The change of absorption was calculated as the glucose concentration of the first samples collected (Period 1) minus the glucose concentration of the last samples collected (Period 2), and expressed as per centimeter perfused bowel. (B) Concentration-dependence of inhibition of glucose absorption by GIP in wild-type mice. Data are shown as means with SEM ($n = 6$ for each group, $P < 0.05$ by ANOVA).

2.7. Analysis

The results are given as mean ± standard error (SEM, n = number of mice). Statistical significance was determined using paired and unpaired Student's t-test and analysis of variance (ANOVA). $P < 0.05$ was considered significant.

3. Results

3.1. Perfusion experiment

Inhibition of glucose absorption was calculated by change in glucose concentration in effluent perfusate in wild-type mice (Fig. 1A). Spontaneous inhibition of glucose absorption of 49 ± 44 nmol/cm/15 min is shown in saline-administered controls (Fig. 1B). Inhibition of glucose absorption was enhanced to 67 ± 40, 163 ± 84, and 409 ± 96 nmol/cm/15 min when the amount of intraperitoneally-administered GIP was increased to 12.5, 25, and 50 nmol/kg body weight, respectively.

3.2. Glucose uptake by jejunum in vitro

We investigated glucose uptake by the jejunum *in vitro* using everted jejunal rings. In the presence of 100 nM GIP in the incubation medium, glucose uptake into jejunal rings in wild-type mice was similar to that in the presence of vehicle (control: 4.2 ± 0.9 μmol/g weight; GIP: 3.5 ± 0.9, P = NS; Fig. 2A). Additionally, glucose uptake into jejunal rings in GIPR$^{-/-}$ mice was similar

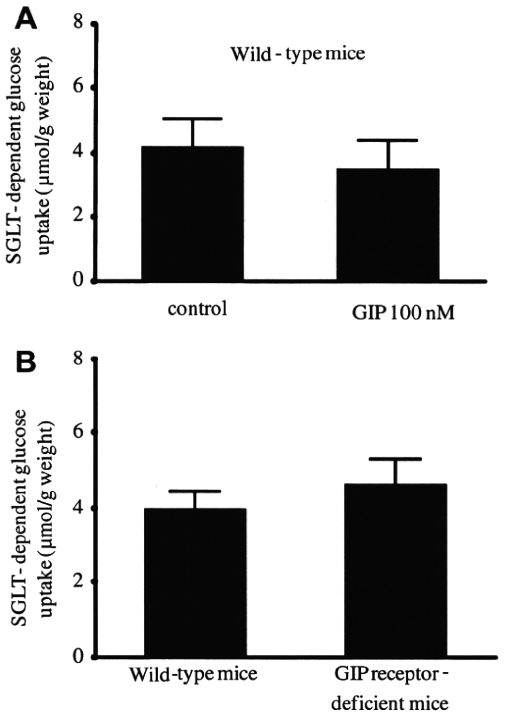

Fig. 2. Glucose uptake in the jejunum. (A) Glucose uptake in the jejunum in wild-type mice in the absence and in the presence of 100 nM GIP. (B) Glucose uptake in the jejunum in wild-type and GIPR$^{-/-}$ mice. SGLT-dependent glucose uptake was determined as the glucose uptake in the absence of 1 mM phlorizin minus the glucose uptake in the presence of 1 mM phlorizin. Data are shown as means with SEM ($n = 8$ for each group).

to that in wild-type mice (wild-type mice: 4.0 ± 0.5 μmol/g weight; GIPR$^{-/-}$ mice 4.6 ± 0.7, P = NS; Fig. 2B).

3.3. Small intestinal transit after intraperitoneal administration of GIP

Intestinal transit rate was measured by the length of small intestine traversed by the charcoal suspension. In wild-type mice, the intestinal transit rate in GIP-administered mice was significantly less than that in saline-administered control (45 ± 8% vs. 68 ± 4%, $P < 0.01$; Fig. 3A). On the other hand, in GIPR$^{-/-}$ mice, the intestinal transit rate was similar to that in saline-administered control and GIP-administered mice (65 ± 3% vs. 63 ± 4%; Fig. 3B).

3.4. Perfusion and intestinal transit in GLP-1 receptor-deficient mice

To determine whether GIP affects intestinal glucose absorption through GLP-1 signaling, inhibition of glucose absorption by GIP was measured in GLP-1R$^{-/-}$ mice. Inhibition of glucose absorption in GLP-1R$^{-/-}$ mice was 44 ± 100 nmol/cm/15 min in saline-administered control mice and 426 ± 104 nmol/cm/15 min in GIP-administered mice (50 nmol/kg body weight, $P < 0.05$, Fig. 3C). Thus, GIP significantly inhibited glucose absorption in GLP-1R$^{-/-}$ mice.

The intestinal transit rate was also evaluated in GLP-1R$^{-/-}$ mice, and was 59 ± 13% in saline-administered control and 42 ± 7% in GIP-administered mice, respectively. Thus, GIP significantly inhibited the intestinal transit rate in GLP-1R$^{-/-}$ mice ($P < 0.01$, Fig. 3D). Consequently, the genetic disruption of GLP-1 receptor did not affect GIP action on intestinal glucose absorption and intestinal transit.

3.5. Involvement of SST in the action of GIP

To determine whether the inhibitory effect of GIP on intestinal transit is due to release of SST, a somatostatin receptor antagonist, CSS (1 μg/kg body weight), was intraperitoneally administered 10 min prior to GIP administration in wild-type mice (Fig. 4A). In the presence of CSS, the intestinal transit rate in GIP-administered wild-type mice was significantly higher than that in the absence of CSS (60 ± 3% vs. 45 ± 8%; $P < 0.01$). Accordingly, CSS reduced the inhibitory effect of GIP on intestinal transit. Moreover, intraperitoneally-administered SST itself significantly inhibited the intestinal transit rate in wild-type mice compared to control (SST: 37 ± 5% vs. control: 68 ± 4%, $P \leqslant 0.01$).

In a perfusion experiment, to confirm that the inhibitory effect of GIP on intestinal glucose absorption is attributable to release of SST, CSS (1 μg/kg body weight) was intraperitoneally administered 10 min prior to GIP administration in wild-type mice (Fig. 4B). In

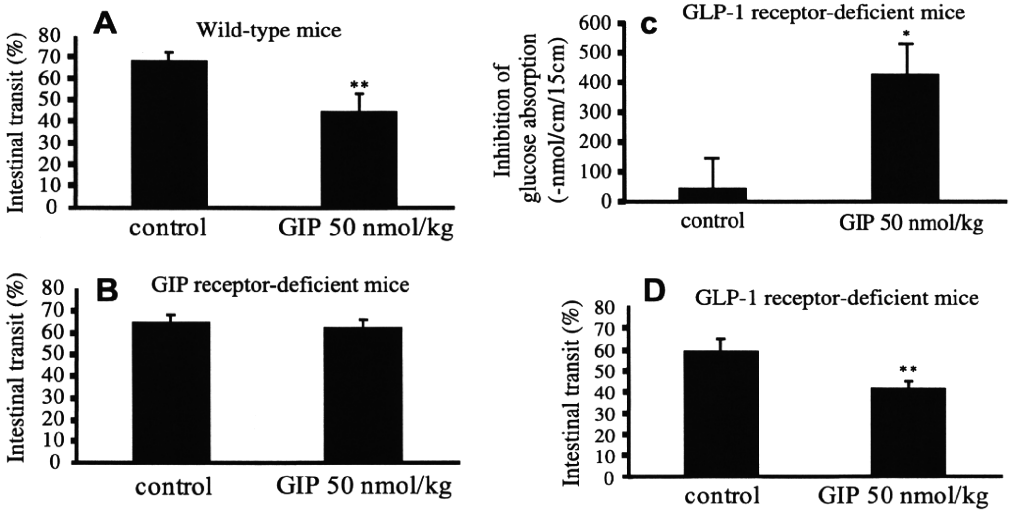

Fig. 3. Intestinal transit after oral administration of non-absorbed marker (10% charcoal suspension in 5% gum Arabic) in wild-type (A) and GIPR$^{-/-}$ (B) mice. Twenty minutes after administration of non-absorbed marker by gavage, the animals were killed and the entire gastrointestinal transit tract was removed. GIP (50 nmol/kg body weight) or saline was administered intraperitoneally 15 min prior to the administration of non-absorbed marker. Data are shown as means with SEM ($n = 6$ for each group). Statistical significance was determined using Student's t-test. **$P < 0.01$ compared with control. (C) Inhibition of glucose absorption in GLP-1R$^{-/-}$ mice with or without intraperitoneal GIP administration as indicated in the legends of Fig 1. (D) Intestinal transit after oral administration of non-absorbed marker in GLP-1R$^{-/-}$ mice with or without intraperitoneal GIP administration as indicated in the legends of Fig 3A. Data are shown as means with SEM ($n = 6$ for each group). Statistical significance was determined using Student's t-test. *$P < 0.05$ compared with control.

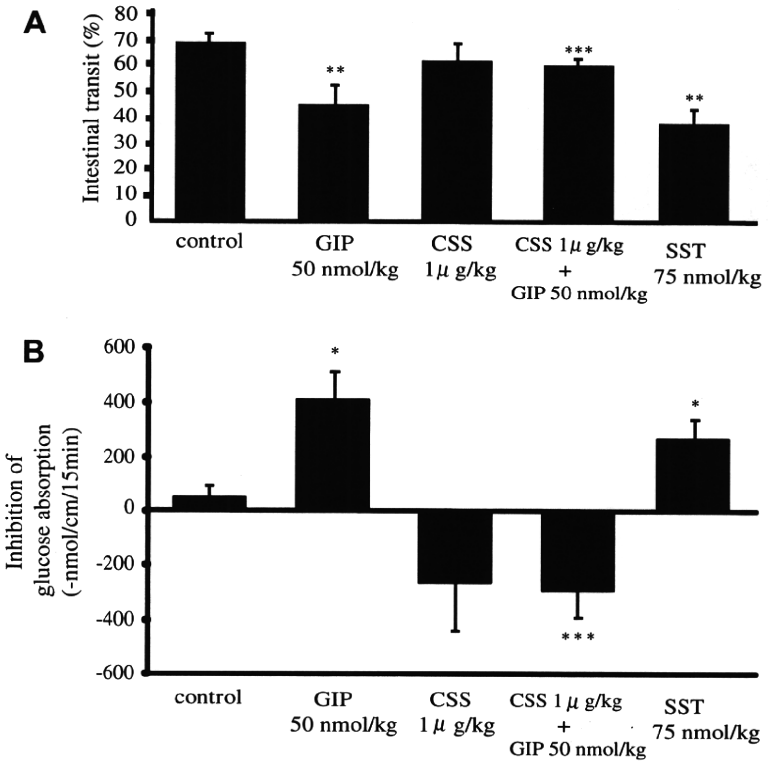

Fig. 4. (A) Intestinal transit after oral administration of non-absorbed marker in wild-type mice with or without pretreatment of CSS. The rate of transit was determined as indicated in the legend of Fig 3A. GIP or SST or saline was administered intraperitoneally 15 min prior to the administration of non-absorbed marker. CSS or saline was intraperitoneally administered 10 min prior to GIP administration. Data are shown as means with SEM ($n = 6$ for each group). Statistical significance was determined using Student's t-test. $^{**}P < 0.01$ compared with control. $^{***}P < 0.01$ compared with GIP alone administered mice. (B) Inhibition of glucose absorption by GIP in wild-type mice with or without pretreatment of CSS, and inhibition of glucose absorption by SST. CSS or saline was intraperitoneally administered 10 min prior to GIP administration. Data are shown as means with SEM ($n = 6$ for each group). Statistical significance was determined using Student's t-test. $^{*}P < 0.05$ compared with control. $^{***}P < 0.01$ compared with GIP alone administered mice.

the presence of CSS, the inhibition of glucose absorption in GIP-administered wild-type mice was significantly lower than that in the absence of CSS (410 ± 96 nmol/cm/15 min vs. −290 ± 99 nmol/cm/15 min; $P < 0.01$). Accordingly, CSS reduced the inhibitory effect of GIP on intestinal glucose absorption. Furthermore, inhibition of glucose absorption in wild-type mice was 49 ± 44 nmol/cm/15 min in saline-administered control mice and 278 ± 63 nmol/cm/15 min in SST-administered mice (75 nmol/kg body weight, $P < 0.05$).

In an experiment of glucose uptake in everted jejunal ring, 100 nM SST did not alter glucose uptake compared to control (control: 4.2 ± 0.9 μmol/g weight; SST: 4.2 ± 0.4, $n = 8$; P = NS).

3.6. Measurement of plasma GIP and SST levels

The plasma levels of total GIP and SST in mice were significantly enhanced 20 min after the intraperitoneal GIP-administration at a dosage of 50 nmol/kg body weight compared to the respective basal levels (GIP: 58 ± 5 pg/ml vs. 3400 ± 257 pg/ml, $n = 8$; $P < 0.01$; SST: 9.9 ± 0.5 ng/ml vs.11.9 ± 0.3 ng/ml, $n = 8$; $P < 0.05$).

4. Discussion

We investigated the inhibitory effect of exogenous GIP on glucose absorption in small intestine. GIP has been known as an important insulinotropic hormone released from duodenal K cells. However, there have been few reports on the effects of GIP on intestinal glucose absorption. In this study, GIP was found to inhibit glucose absorption in a concentration-dependent manner by the perfusion method.

Glucose absorption includes two steps in enterocytes, permeation through brush-border membrane and subsequently through basolateral membrane. Glucose and galactose cross the brush-border membrane by means of SGLT-1, which is a rate-limiting step of glucose absorption [10]. Recent *in vitro* study by Singh et al. found that exogenous GIP stimulates SGLT-dependent glucose absorption by using an Ussing chamber experiment [11]. In the experiment, intestine was fixed between two chambers, and short-circuit-current representing SGLT activity was measured. However, in our experiments using everted jejunal rings, which is another method to measure SGLT-dependent glucose absorption *in vitro*, the lack of effect of exogenous GIP on SGLT-dependent glucose uptake was shown, and genetic disruption of the GIP receptor was found not to affect SGLT-dependent glucose absorption. The reason why our results and theirs are different is unknown, but may be attributable to difference in method.

It is generally accepted that there is a positive relationship between intestinal motility and absorption [4,5]. It has been shown that increased intestinal motility, besides enhancing the functional surface area, facilitates diffusion of glucose to the transporters of the brush-border membrane by altering the unstirred water layer [12,13]. We investigated the effect of GIP on motility of small intestine by evaluating intestinal transit. In this study, GIP was found to inhibit intestinal transit compared to control in wild-type but not in $GIPR^{-/-}$ mice. Thus, the inhibitory effect of GIP on glucose absorption may be attributable, in part, to inhibition of intestinal motility.

GLP-1, another incretin hormone, is secreted from L cells found predominantly in ileal mucosa, and is known to be part of the "ileal brake" that acts as an inhibitor of upper gastrointestinal motility

[14]. In this study, GIP was found to inhibit intestinal transit in GLP-1R$^{-/-}$ mice as well as in wild-type mice, indicating that the inhibitory action of GIP on gastrointestinal transit is not mediated by GLP-1. Furthermore, glucose absorption was found to be inhibited significantly by GIP in GLP-1R$^{-/-}$ mice as well as in wild-type mice, suggesting that the primary mechanism of the inhibition of intestinal glucose absorption by GIP most likely does not involve the GLP-1-mediated pathway.

Recently, Miki et al. reported that GLP-1 inhibited gut motility while GIP did not [15]. In this study, however, GIP was found to inhibit intestinal transit. The inconsistency could be due to their use of a non-absorbed marker containing a high concentration (as much as 50%) of glucose to evaluate gut motility, whereas we used a non-absorbed marker without glucose. Intraduodenal infusion of hyperosmolar solution was reported to increase duodenal motility, which is mediated by activation of osmoreceptors in duodenum [16]. In our preliminary experiment on small intestinal transit using 10% charcoal suspension in 5% gum Arabic with 50% glucose, the intestinal transit rate was significantly greater than that when using glucose-free solution (88 ± 8% vs. 68 ± 4%, $P < 0.05$, unpublished data). Therefore, intestinal transit might be enhanced by the high concentration of glucose itself in the suspension, which could conceal a GIP-evoked inhibitory effect on intestinal transit. However, limitations of this study must be considered. While GIP was found to inhibit intestinal transit under the conditions of this study, the effect of GIP on intestinal transit may differ among the constituents of the food or nutrient. Further investigations are required.

Regarding the GIP dosage applied in the *in vivo* experiments, low GIP dosage has been used when applied by the route of continuous intravenous administration; GIP (0.25 nmol/kg body weight) was reported to stimulate insulin secretion by intravenous administration in rat [17] and (GIP 4 pmol/kg body weight/min) in human [18]. However, high GIP dosage has been used when applied by the other routes of administration than intravenous administration. Indeed, one group has reported that subcutaneous pre-administration of 100 μg GIP (approximately 800 nmol/kg body weight) lowered glucose excursion in oral glucose tolerance test in mice [15] and another group has reported that intraperitoneal administration of [D-Ala^2]GIP (48 nmol/kg body weight/day), a DPP4-resistant analogue, lowered glucose excursion in intraperitoneal glucose tolerance test in mice [19]. In this study, we applied GIP intraperitoneally at a dosage of 50 nmol/kg body weight to demonstrate the pharmacological effects of GIP on intestinal transit and glucose absorption, which dosage is comparable to those used in the latter reports.

Regarding the mechanism of inhibition of intestinal transit by GIP, SST secretion has been reported to be stimulated by GIP [20–22] and to prolong intestinal transit [23,24]. The SST receptor has five isoforms (sst1-5) and all five receptors have been shown to be expressed in gastrointestinal tract, with high levels of sst2 receptor in intestine [25]. The sst2 receptors in intestine have been shown not to be expressed on enterocytes or muscle cells, but on myenteric and submucosal plexuses and on neuroendocrine cells in epithelium [26] and also on interstitial cells of Cajal in deep muscular plexus [27]. Thus, the mechanisms by which exogenous GIP inhibits intestinal motility through two SST-mediated pathways may be as follows. In the first, exogenous GIP binds to the GIP receptors on the cell surface membrane in SST-containing enteric neurons and/or in mucosal endocrine cells of D cells in gastrointestinal tract and/or in pancreatic islets, resulting in the release of SST. Subsequently, the released SST acts as a neurotransmitter and binds to sst2 receptors expressed on other neurons in myenteric plexus, parts of which nerve fibers are distributed to muscular cells, permitting inhibition of intestinal motility. In this pathway, the local SST concentration in interneural synaptic space may be increased prominently. In an alternate pathway, SST secreted from D cells flows into systemic circulation through submucosal vessels to reach the neurons in myenteric plexus. Indeed, in this study, intraperitoneally-administered GIP induced a small but significant increase in plasma SST levels, suggesting involvement of the latter pathway.

In our experiment of intestinal perfusion, GIP was found to inhibit intestinal glucose absorption primarily by reducing intestinal motility. On the other hand, the tissue of everted intestinal ring is set inside-out and distended far from the physiological condition, and thus incapable of reflecting general intestinal motility. Thus, the lack of GIP action on glucose uptake in the tissues of everted intestinal ring in this study may be expected.

Several studies have found that the inhibitory effect of SST on intestinal glucose absorption may be attributable to either the effect of SST on the splanchnic hemodynamics [28] or a direct effect of SST on enterocytes [29]. However, consistent with this study, another study has found that SST delays intestinal glucose absorption by its inhibitory effect on intestinal motility [24]. SST exerts its inhibitory effect on intestinal glucose absorption by several mechanisms; our results indicate that the inhibitory effect of SST is mediated, at least in part, by alteration of intestinal motility.

In this study, the somatostatin receptor antagonist CSS was found to reduce the inhibitory effect of GIP on intestinal transit, suggesting that GIP stimulates SST release. In addition, we show that SST itself inhibits intestinal transit and glucose absorption in perfused intestine. Consistently, a recent study has reported that SST inhibits intestinal glucose absorption [29]. Considered together with previous reports, we conclude that exogenous GIP inhibits intestinal transit and glucose absorption indirectly through a somatostatin-mediated pathway.

One of the physiological roles of GIP is known to be facilitation of nutrient uptake into adipose tissue and bone. In this study, exogenous GIP was found to inhibit intestinal glucose absorption by reducing intestinal motility. Since this observation was obtained by the action of a supraphysiological level of plasma GIP, it is unclear whether or not the action is associated with already known physiological actions of GIP. In the point of delay of intestinal carbohydrate absorption, however, the biological action of GIP found in this study appears to be similar to that of medical medicine α-glucosidase inhibitor, which does not influence the regulation of energy accumulation in adipose tissue or bone.

Acknowledgments

This study was supported by Scientific Research Grants and a Grant for Leading Project for Biosimulation from the Ministry of Education, Culture, Sports, Science, and Technology of Japan, a grant from CREST of Japan Science and Technology Cooperation, and a grant from the Ministry of Health, Labor, and Welfare, Japan, and also by Kyoto University Global COE Program "Center for Frontier Medicine". The authors are grateful to Dr. Daniel J. Drucker for kindly providing GLP-1R$^{-/-}$ mice.

References

[1] Y. Seino, M. Fukushima, D. Yabe, GIP and GLP-1, the two incretin hormones: similarities and differences, J. Diabetes Invest. 1 (2010) 8–23.
[2] K. Miyawaki, Y. Yamada, H. Yano H, et al., Glucose intolerance caused by a defect in the entero-insular axis: a study in gastric inhibitory polypeptide receptor knockout mice, Proc. Natl. Acad. Sci. USA 96 (1999) 14843–14847.
[3] T.B. Usdin, E. Mezey, D.C. Button, et al., Gastric inhibitory polypeptide receptor, a member of the secretin-vasoactive intestinal peptide receptor family, is widely distributed in peripheral organs and the brain, Endocrinology 133 (1993) 2861–2870.
[4] M. Sababi, U.H. Bengtsson, Enhanced intestinal motility influences absorption in anaesthetized rat, Acta Physiol. Scand. 172 (2001) 115–122.
[5] A.J. Smout, Small intestinal motility, Curr. Opin. Gastroenterol. 20 (2004) 77–81.

[6] L.A. Scrocchi, T.J. Brown, N. MaClusky, et al., Glucose intolerance but normal satiety in mice with a null mutation in the glucagon-like peptide 1 receptor gene, Nat. Med. 2 (1996) 1254–1258.
[7] R. Athman, A. Tsocas, O. Presset, et al., In vivo absorption of water and electrolytes in mouse intestin, Application to villin$^{-/-}$ mice, Am. J. Physiol. Gastrointest. Liver Physiol. 282 (2002) G634–639.
[8] K. Tsukiyama, Y. Yamada, K. Miyawaki, et al., Gastric inhibitory polypeptide is the major insulinotropic factor in K(ATP) null mice, Eur. J. Endocrinol. 151 (2004) 407–412.
[9] K. Yamada, M. Hosokawa, S. Fujimoto, et al., The spontaneously diabetic Torii rat with gastroenteropathy, Diabetes Res. Clin. Pract. 75 (2007) 127–134.
[10] M.A. Hediger, M.J. Coady, T.S. Ikeda, et al., Expression cloning and cDNA sequencing of the Na^+/glucose co-transporter, Nature 330 (1987) 379–381.
[11] S.K. Singh, A.C. Bartoo, S. Krishnan, et al., Glucose-dependent insulinotropic polypeptide (GIP) stimulates transepithelial glucose transport, Obesity 16 (2008) 2412–2416.
[12] F.A. Wilson, J.M. Dietschy, The intestinal unstirred layer: its surface area and effect on active transport kinetics, Biochim. Biophys. Acta 363 (1974) 112–126.
[13] D.V. Rayner, The relationships between glucose absorption and insulin secretion and the migrating myoelectric complex in the pig, Exp. Physiol. 76 (1991) 67–76.
[14] A. Wettergren, B. Schjoldager, P.E. Mortensen, et al., Truncated GLP-1 (proglucagon 78–107-amido) inhibits gastric and pancreatic functions in man, Dig. Dis. Sci. 38 (1993) 665–673.
[15] T. Miki, K. Minami, H. Shinozaki, et al., Distinct effects of glucose-dependent insulinotropic polypeptide and glucagon-like peptide-1 on insulin secretion and gut motility, Diabetes 54 (2005) 1956–1963.
[16] H.C. Lin, J.D. Elashoff, G.M. Kwok, et al., Stimulation of duodenal motility by hyperosmolar mannitol depends on local osmoreceptor control, Am. J. Physiol. 266 (1994) G940–943.
[17] E.L. Mazzaferri, L. Ciofalo, L.A. Waters, et al., Effects of gastric inhibitory polypeptide on leucine- and arginine-stimulated insulin release, Am. J. Physiol. 245 (1983) E114–E120.
[18] T. Vilsbøll, T. Krarup, S. Madsbad, et al., Defective amplification of the late phase insulin response to glucose by GIP in obese Type II diabetic patients, Diabetologia 45 (2002) 1111–1119.
[19] B.J. Lamont, D.J. Drucker, Differential antidiabetic efficacy of incretin agonists versus DPP-4 inhibition in high fat fed mice, Diabetes 57 (2008) 190–198.
[20] J. Szecówka, V. Grill, E. Sandberg, et al., Effect of GIP on the secretion of insulin and somatostatin and the accumulation of cyclic AMP in vitro in the rat, Acta Endocrinol. (Copenh) 99 (1982) 416–421.
[21] L. Hansen, J.J. Holst, The effects of duodenal peptides on glucagon-like peptide-1 secretion from the ileum. A duodeno–ileal loop?, Regul Pept. 110 (2002) 39–45.
[22] J.J. Holst, S.L. Jensen, S. Knuhtsen, et al., Effect of vagus, gastric inhibitory polypeptide, and HCl on gastrin and somatostatin release from perfused pig antrum, Am. J. Physiol. 244 (1983) G515–522.
[23] G.J. Krejs, Effect of somatostatin and absorption and atropine infusion on intestinal transit tine and fructose absorption in the perfused human jejunum, Diabetes 33 (1984) 548–551.
[24] C. Johansson, O. Wisén, S. Efendić, et al., Effects of somatostatin on gastrointestinal propagation and absorption of oral glucose in man, Digestion 22 (1981) 126–137.
[25] K. Krempels, B. Hunyady, A.M. O'Carroll, et al., Distribution of somatostatin receptor messenger RNAs in the rat gastrointestinal tract, Gastroenterology 112 (1997) 1948–1960.
[26] M. Gugger, B. Waser, A. Kappeler, et al., Cellular detection of sst2A receptors in human gastrointestinal tissue, Gut 53 (2004) 1431–1436.
[27] C. Sternini, H. Wong, S.V. Wu, et al., Somatostatin 2A receptor is expressed by enteric neurons, and by interstitial cells of Cajal and enterochromaffin-like cells of the gastrointestinal tract, J. Comp. Neurol. 386 (1997) 396–408.
[28] J. Wahren, Influence of somatostatin on carbohydrate disposal and absorption in diabetes mellitus, Lancet 2 (1976) 1213–1216.
[29] F. Féry, L. Tappy, P. Schneiter, et al., Effect of somatostatin on duodenal glucose absorption in man, J. Clin. Endocrinol. Metab. 90 (2005) 4163–4169.

nature COMMUNICATIONS

OPEN

ARTICLE

Received 6 Aug 2010 | Accepted 27 Oct 2010 | Published 23 Nov 2010

DOI: 10.1038/ncomms1127

Disruption of TBP-2 ameliorates insulin sensitivity and secretion without affecting obesity

Eiji Yoshihara[1,2], Shimpei Fujimoto[3], Nobuya Inagaki[3], Katsuya Okawa[4], So Masaki[1], Junji Yodoi[1] & Hiroshi Masutani[1]

Type 2 diabetes mellitus (T2DM) is characterized by defects in both insulin sensitivity and glucose-stimulated insulin secretion (GSIS) and is often accompanied by obesity. In this study, we show that disruption of thioredoxin binding protein-2 (TBP-2, also called Txnip) in obese mice (ob/ob) dramatically improves hyperglycaemia and glucose intolerance, without affecting obesity or adipocytokine concentrations. TBP-2-deficient ob/ob mice exhibited enhanced insulin sensitivity with activated insulin receptor substrate-1/Akt signalling in skeletal muscle and GSIS in islets compared with ob/ob mice. The elevation of uncoupling protein-2 (UCP-2) expression in ob/ob islets was downregulated by TBP-2 deficiency. TBP-2 overexpression suppressed glucose-induced adenosine triphosphate production, Ca^{2+} influx and GSIS. In β-cells, TBP-2 enhanced the expression level and transcriptional activity of UCP-2 by recruitment of peroxisome proliferator-activated receptor-γ co-activator-1α to the UCP-2 promoter. Thus, TBP-2 is a key regulatory molecule of both insulin sensitivity and GSIS in diabetes, raising the possibility that inhibition of TBP-2 may be a novel therapeutic approach for T2DM.

[1] Department of Biological Responses, Institute for Virus Research, Kyoto University, Kyoto 606-8507, Japan. [2] Division of Systemic Life Science, Graduate School of Biostudies, Kyoto University, Kyoto 606-8501, Japan. [3] Department of Diabetes and Clinical Nutrition, Faculty of Medicine, Kyoto University, Kyoto 606-8507, Japan. [4] Drug Discovery Research Laboratories, Kyowa Hakko Kirin Co. Ltd, Shizuoka 411-8731, Japan. Correspondence and requests for materials should be addressed to H.M. (email: hmasutan@virus.kyoto-u.ac.jp).

Regulation of glucose homeostasis is critical to life in mammals and is largely maintained by pancreatic β-cells, which secrete insulin in response to increased concentrations of glucose, and is also maintained by the glucose uptake response to insulin in peripheral tissues. Obesity disrupts glucose homeostasis and leads to diseases such as type 2 diabetes (T2DM), which is characterized by aggravated insulin sensitivity and insulin secretion[1–5].

Thioredoxin binding protein-2 (TBP-2), also known as thioredoxin interacting protein (Txnip)[6] and vitamin-D3 upregulated protein-1 (VDUP1)[7], has been identified as a negative regulator of thioredoxin and is mainly localized in the nucleus[8,9]. TBP-2 is a member of the α-arrestin protein family, and contains two characteristic arrestin-like domains and two PPxY sequences, which is a known binding motif for WW domain containing proteins[10–12]. Evidence is growing that TBP-2 has an important role in a wide variety of biological functions, such as the regulation of cell death, cell growth, cell differentiation, immune responses and energy metabolism[13–22]. As our group and others have shown that TBP-2-deficient mice or mice carrying the TBP-2 nonsense mutation (HcB-19) have increased insulin sensitivity[16,20,23] and insulin secretion[16,18], we hypothesized that TBP-2 is involved in defects of insulin sensitivity and secretion in diabetes.

In this study, to address the physiological and molecular role of TBP-2 in diabetes, we generated a TBP-2-deficient diabetic mice model (ob/ob·TBP-2 − / −). Remarkably, these mice displayed improved glucose intolerance due to enhanced muscle insulin sensitivity associated with the insulin receptor substrate-1 (IRS-1)/Akt pathway and glucose-stimulated insulin secretion (GSIS) in spite of obesity. The augmented insulin secretion was due to the elevation of glucose-induced adenosine triphosphate (ATP) production with suppression of mitochondrial uncoupling protein-2 (UCP-2) expression. UCP-2 is known as a negative regulator of GSIS in diabetes[24]. We showed that TBP-2 regulates insulin secretion mainly through UCP-2 transcriptional activation in β-cell lines. We further investigated mechanisms for TBP-2 regulation of UCP-2 transcription and analysed interacting proteins for TBP-2 in β-cells. The current results provide a novel mechanism for elucidating the pathogenesis of diabetes.

Results

Disruption of TBP-2 in ob/ob mice improves hyperglycaemia. Subsequent to a report that TBP-2 expression is elevated in skeletal muscle of patients with impaired glucose tolerance or T2DM[19], we examined the expression levels of TBP-2 mRNA in the tissues of leptin-deficient (ob/ob) mice; a genetic animal model of human obesity and T2DM. Expression levels of TBP-2 were increased in the heart, skeletal muscle, white adipose tissue, kidney and pancreatic islets, but were not significantly changed in the liver of ob/ob mice compared with wild-type (WT) lean mice (Fig. 1a). To determine how TBP-2 is involved in the development of diabetic phenotypes in obese mice, we next studied the effect of endogenous TBP-2 in ob/ob mice by generating TBP-2-deficient ob/ob mice (ob/ob·TBP-2 − / −) (Fig. 1b). Ob/ob·TBP-2 − / − mice did not show any significant change in food intake, but showed reduced water intake compared with that of ob/ob mice (Fig. 1c,d). Surprisingly, although body weight was higher in male and as high in female ob/ob·TBP-2 − / − mice compared with that in ob/ob mice (Fig. 1e,g), TBP-2 deficiency markedly improved hyperglycaemia and urinary glucose excretion both in male and female ob/ob mice (Fig. 1f,h,i). Furthermore, glucose tolerance tests revealed significant amelioration of glucose metabolism in ob/ob·TBP-2 − / − mice (Fig. 1j,k), consistent with insulin tolerance tests (ITTs) in which insulin sensitivity significantly increased in ob/ob·TBP-2 − / − mice compared with that in ob/ob mice (Fig. 1l,m). These results suggest that disruption of TBP-2 in ob/ob mice improves glucose tolerance and insulin sensitivity.

TBP-2 deficiency ameliorates insulin resistance. As altered production of adipocytokines accompanied with obesity is implicated in insulin resistance and glucose intolerance[2,25], body fat composition, serum monocyte chemotactic protein-1 (MCP-1), adiponectin and metabolic parameters of ob/ob·TBP-2 − / − mice were measured. In ob/ob·TBP-2 − / − mice, body fat and serum levels of fatty acids, MCP-1 and lipids increased and serum adiponectin decreased compared with those in WT and/or ob/ob mice (Fig. 2a–i and Supplementary Table S1). TBP-2 deficiency in ob/ob mice did not improve adipose size, and TBP-2 − / − mice showed increased adipose size compared with that in WT mice (Fig. 2j). These results show that TBP-2 deficiency improves insulin sensitivity without amelioration of overeating, obesity and adipocyte dysfunction.

As insulin resistance is derived from defects in insulin signalling in peripheral tissues,[1] and insulin/Akt signalling regulates many of the metabolic actions of insulin[1], we investigated phosphorylation of Akt in these mice. Akt phosphorylation levels in both basal- and insulin-stimulated states were upregulated in skeletal muscle, heart and liver of TBP-2 − / − mice compared with those in WT mice (Fig. 2k–p). In addition, TBP-2 deficiency enhanced Akt phosphorylation levels in response to insulin in mouse embryonic fibroblasts (MEFs) (Fig. 2q,r), suggesting that TBP-2 deficiency enhances insulin/Akt signalling. Although ob/ob mice showed suppression of Akt phosphorylation in response to insulin in skeletal muscle, heart and liver, compared with those in WT mice without affecting the concentration of total Akt protein, TBP-2 deficiency in ob/ob mice restored the suppression of Akt phosphorylation in skeletal muscle and heart, but not liver (Fig. 2k–p). The phosphorylation of FoxO1, an Akt downstream signalling molecule, was also not enhanced in the liver of ob/ob·TBP-2 − / − mice. Severe lipid accumulation occurred in the liver both in ob/ob and ob/ob·TBP-2 − / − mice (Supplementary Fig. S1a,b). Thus, the amelioration of insulin sensitivity by TBP-2 deficiency in ob/ob mice seems to be due to activation of insulin/Akt signalling in skeletal muscle.

TBP-2 deficiency enhances IRS-1 expression in skeletal muscle. We performed microarray analyses (data deposited in GEO, accession number GSE24851) of the skeletal muscle in WT, TBP-2 − / − , ob/ob, ob/ob·TBP-2 − / − mice to investigate how TBP-2 regulates Akt signalling and insulin sensitivity. We found that several insulin signalling-related genes, such as *Igf1, Igf2bp2, Igfbp4, Irs-1(IRS-1), Pik3r1* and *Pik3r5*, were upregulated by TBP-2 deficiency both in WT and ob/ob background mice (Supplementary Table S2). The upregulation was confirmed by real-time reverse transcription (RT)–PCR analyses (Fig. 3a). *IRS-1* gene expression was downregulated in skeletal muscle of ob/ob mice (Fig. 3a) or T2DM patients[26]. We focused on IRS-1, as IRS-1 is one of the key molecules for insulin signalling and is an upstream molecule of Akt in skeletal muscle[27]. IRS-1 protein levels were downregulated in ob/ob mice, whereas IRS-1 protein levels and phosphorylation of Akt were upregulated by TBP-2 deficiency in skeletal muscle of WT and ob/ob background mice (Fig. 3b). Thus, TBP-2 regulates the expression of molecules involved in insulin signalling, which may enhance insulin sensitivity in skeletal muscle. Gene expressions of peroxisome proliferator-activated receptor (PPAR) signalling were also enhanced by TBP-2 deficiency in skeletal muscle (Supplementary Fig.S2).

TBP-2 deficiency improved impairment of insulin secretion. TBP-2 − / − mice and HcB-19 mice show enhanced insulin secretion *in vivo*[16,18]. Although obesity usually leads to insulin resistance, only a subset of obese- and insulin-resistant individuals progress to T2DM. In ob/ob mice and humans, the determinant factor for declining glucose tolerance is a progressive decrease in GSIS[3]. Of note, ob/ob mice showed elevated blood glucose with an increase in body weight after ages 5 or 6 weeks, whereas TBP-2-deficient ob/ob mice did not show elevation of blood glucose, in spite of similar increases in body weight. In addition, although blood glucose levels

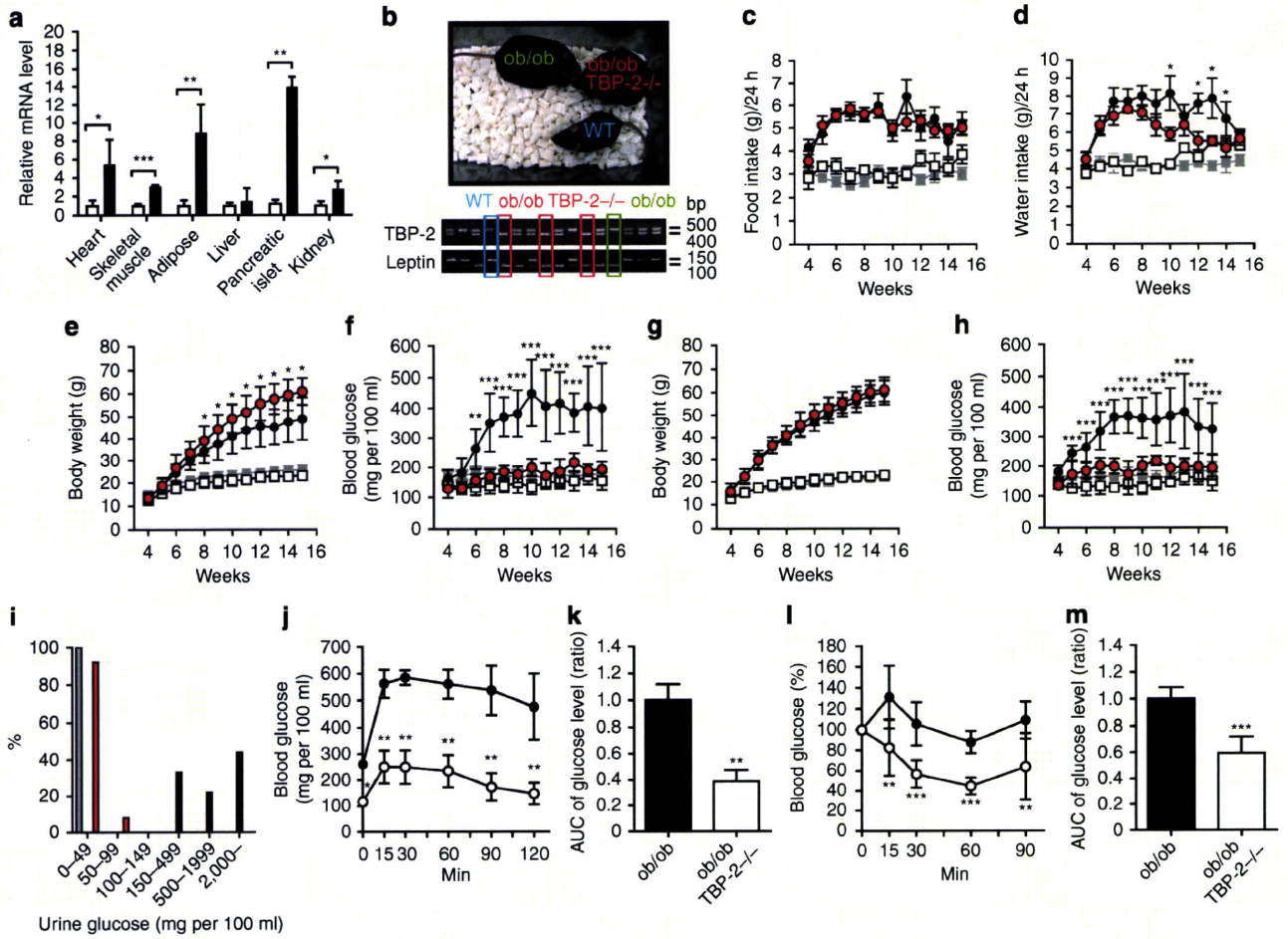

Figure 1 | Disruption of TBP-2 in ob/ob mice improves hyperglycaemia and glucose intolerance without affecting obesity. (**a**) Quantitative RT-PCR of *TBP-2* expression in the heart, skeletal muscle, white adipose, liver, pancreatic islet and kidney of WT (open bar, lean, $n=3$) and ob/ob mice (closed bar, $n=3$). (**b**) Generation of the ob/ob·TBP-2−/− mice. Male food intake (**c**), male water intake (**d**), male body weight (**e**), male blood glucose in fed *ad lib* (**f**), female body weight (**g**), female blood glucose in fed *ad lib* (**h**) were assessed, $N \geq 6$. WT, grey rectangles; TBP-2−/−, white rectangles; ob/ob, black circles; ob/ob·TBP-2−/−, red circles. (**i**) Urine glucose (mg per 100 ml) of males and females. WT (grey bar; $n=11$), ob/ob (black bar; $n=9$), ob/ob·TBP-2−/− (red bar; $n=11$). (**j**, **k**) Intraperitoneal glucose tolerance test (IPGTT). Following an overnight fast, mice were injected with 0.5 g kg^{-1} glucose, IP (time 0). Blood glucose values (**j**) and area under the curve (AUC) levels (**k**) were assessed before and at 15, 30, 60 and 120 min into the IPGTT. ob/ob (black circle, $n=5$), ob/ob·TBP-2−/− (white circle, $n=6$). (**l**, **m**) IP insulin tolerance test (IPITT). Following a 6 h fast, mice were injected with 1 U/kg of insulin, i.p. (time 0). Blood glucose value (**l**) and AUC levels (**m**) were assessed before and at 15, 30, 60 and 90 min into the IPITT. ob/ob (black circle, $n=5$), ob/ob·TBP-2−/− (white circle, $n=6$). Data are presented as mean±s.d. $^*P<0.05$, $^{**}P<0.01$, $^{***}P<0.001$, versus control (*t*-test).

were lower in ob/ob·TBP-2−/− mice, compared with those in ob/ob mice, serum insulin levels in ob/ob·TBP-2−/− mice were as high as those in ob/ob mice at ages 11 and 14 weeks in both males and females (Fig. 4a,b). Although we observed no significant change in islet mass between ob/ob·TBP-2−/− mice and ob/ob mice, as well as between TBP-2−/− and WT mice (Fig. 4c,d), serum insulin levels after glucose loads *in vivo* were enhanced in ob/ob·TBP-2−/− mice compared with those in ob/ob mice (Fig. 4e). To evaluate the effect of TBP-2 deficiency on insulin secretion *ex vivo*, pancreatic islets were isolated from WT, TBP-2−/−, ob/ob and ob/ob·TBP-2−/− mice. TBP-2 deficiency enhanced GSIS in both WT and ob/ob mice (Fig. 4f,g). Insulin secretion from ob/ob islets in response to high glucose was blunted, and was improved by TBP-2 deficiency (Fig. 4g,h). These results suggest that TBP-2 deficiency improves impairment of GSIS from islets, which contributes to improvement of glucose intolerance in ob/ob mice. As glucose metabolism generates ATP as a signal to enhance insulin secretion[28], we further determined ATP content of islets in these mice. Under a high (16.7 mM) glucose condition, TBP-2 deficiency enhanced ATP content in both WT and ob/ob islets (Fig. 4i,j). WT islets showed a significant increase in ATP production with increased glucose concentrations (Fig. 4i). In ob/ob islets, increases in ATP content with increasing glucose levels were not as marked (Fig. 4j,k), as in TBP-2 deficiency where the ratio of ATP content at high glucose (16.7 mM) relative to basal glucose (2.8 mM) was significantly increased (Fig. 4k). Regulation of mitochondrial ATP production has a central role in insulin secretion from pancreatic β-cells[4], and the reduction of mitochondrial ATP production parallels abnormal mitochondrial structure, including swelling and alteration in volume density and cristae structure[29], which is often observed in diabetes[5,30]. We then studied the morphology of mitochondria in WT, TBP-2−/−, ob/ob and ob/ob·TBP-2−/− β-cells using electron microscopy. Morphological apoptotic processes, including condensation of chromatin around the nuclear membrane and swelling of the cytoplasm and a decrease in the number of insulin granules in β-cells, were not observed in ob/ob and ob/ob·TBP-2−/− mice at 10 weeks ages (Supplementary Fig. S3a,b). However, the abnormal mitochondrial morphological changes, such as swelling associated with an increased number of disarrayed or disappeared cristae and a reduced electron density of the matrix, were observed in ob/ob mice, whereas the abnormalities were improved in ob/ob·TBP-2−/− mice

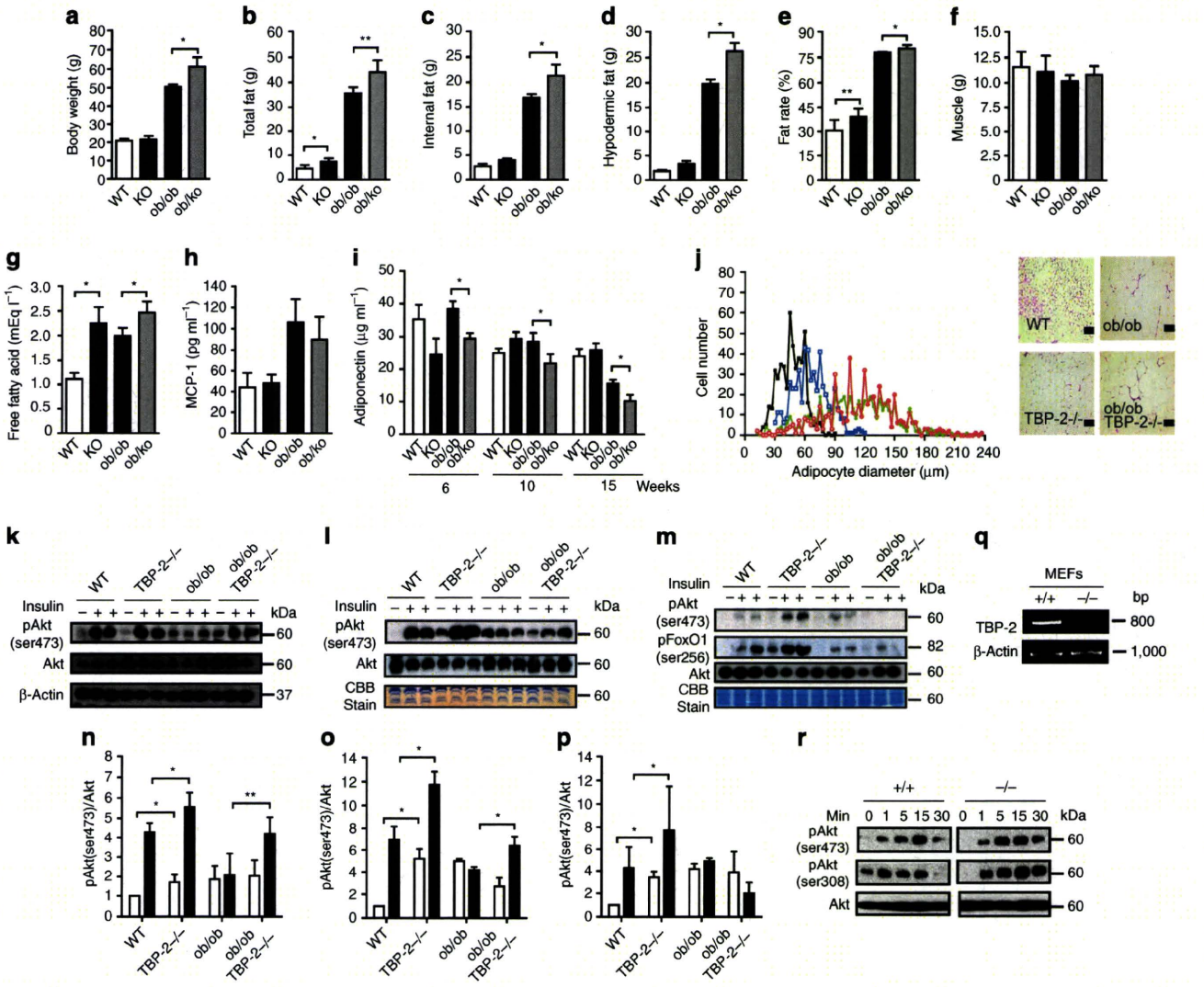

Figure 2 | TBP-2 deficiency ameliorates insulin resistance and increase Akt signalling. (**a**–**f**) Fat and muscle content. Body weight (**a**), total fat (**b**), internal fat (**c**), hypodermic fat (**d**), fat rate (**e**), muscle (**f**) in male WT (WT), TBP-2−/− (KO), ob/ob (ob/ob) and ob/ob·TBP-2−/− (ob/ko) mice calculated from computed tomography scan data are shown for 15 weeks aged mice, $N \geq 4$. (**g**, **h**) Serum physiological parameters. Free fatty acid (**g**) and MCP-1 (**h**) were measured in 15 weeks aged mice, $N \geq 7$. (**i**) Blood adiponectin concentration was measured in 6, 10 and 15 weeks aged mice, $n = \geq 5$. (**j**) Distribution of adipocyte size in white adipose from 10 weeks aged WT (black closed rectangle), TBP-2−/− (blue open rectangle), ob/ob (green closed circle) and ob/ob·TBP-2−/− (red open circle) mice (left panel). The right panel shows histological analyses of haematoxylin and eosin (HE)-stained white adipose sections in these mice. Scale bar indicates 100 μm. (**k**–**m**) Immuno blotting (IB) analyses of ser473-phospholylated Akt (pAkt), ser256-phospholylated FoxO1 (pFoxO1) and total Akt in response to insulin (2 U kg^{-1}) in skeletal muscle (**k**), heart (**l**) and liver (**m**). Densitometric quantification of pAkt/Akt ratios in skeletal muscle (**n**), heart (**o**) and liver (**p**). Open and closed bar represents without or with insulin stimulation, respectively. (**q**) Loss of endogenous TBP-2 mRNA in MEFs. (**r**) IB analyses. TBP-2 deficiency enhances insulin/Akt signalling in primary MEFs. MEFs were serum starved for 12 h and then stimulated with insulin (100 nM) for different times. Data are presented as mean±s.d. *P< 0.05, **P< 0.01, versus control (t-test).

(Fig. 4l). These results showed that mitochondrial morphological changes and metabolic dysfunctions in β-cells are improved by TBP-2 deficiency in ob/ob mice.

TBP-2 suppresses mitochondrial ATP production and GSIS. To delineate how TBP-2 deficiency protects against the impaired GSIS in ob/ob islets, we next examined the dose effect of TBP-2 on GSIS in the rat β-cell line INS-1 cells. Silencing of TBP-2 (RNAi1 and RNAi2) enhanced GSIS in INS-1 cells (Fig. 5a,b,d). On the contrary, transient TBP-2 overexpression suppressed GSIS (Fig. 5c,e). Induction of TBP-2 in cloned INS-1 cells, where TBP-2 expression was doxycycline-off dependent, suppressed GSIS, but not KCl-induced insulin secretion (Fig. 5f,g). TBP-2 induction did not cause a significant change in ATP levels at low (2.8 mM) glucose level, but it suppressed ATP levels at high (16.7 mM) glucose in INS-1 cells (Fig. 5h). Furthermore, glucose-induced intracellular Ca^{2+} elevation, which is the eventual trigger for the exocytosis of insulin granules, was significantly decreased in TBP-2-induced INS-1 cells (Fig. 5i). We then analysed mitochondrial membrane potentials ($\Delta\psi_m$) in TBP-2-induced INS-1 cells. We showed that $\Delta\psi_m$ was significantly reduced in TBP-2-induced INS-1 cells cultured with low (3 mM) and high (20 mM) glucose (Fig. 5j) and with 11 mM glucose for 24 h (Fig. 5k) using a flowcytometer and fluorescence microscopy, respectively. Cellular ATP is mainly produced by glycolysis and mitochondrial metabolism. In pancreatic β-cells, glycolytic flux regulates glucose metabolism, which has an important role in insulin secretion, and glucokinase is a pace-setting enzyme in glycolysis[31]. Therefore, effects of TBP-2 on glucokinase activity were examined. Glucokinase activity

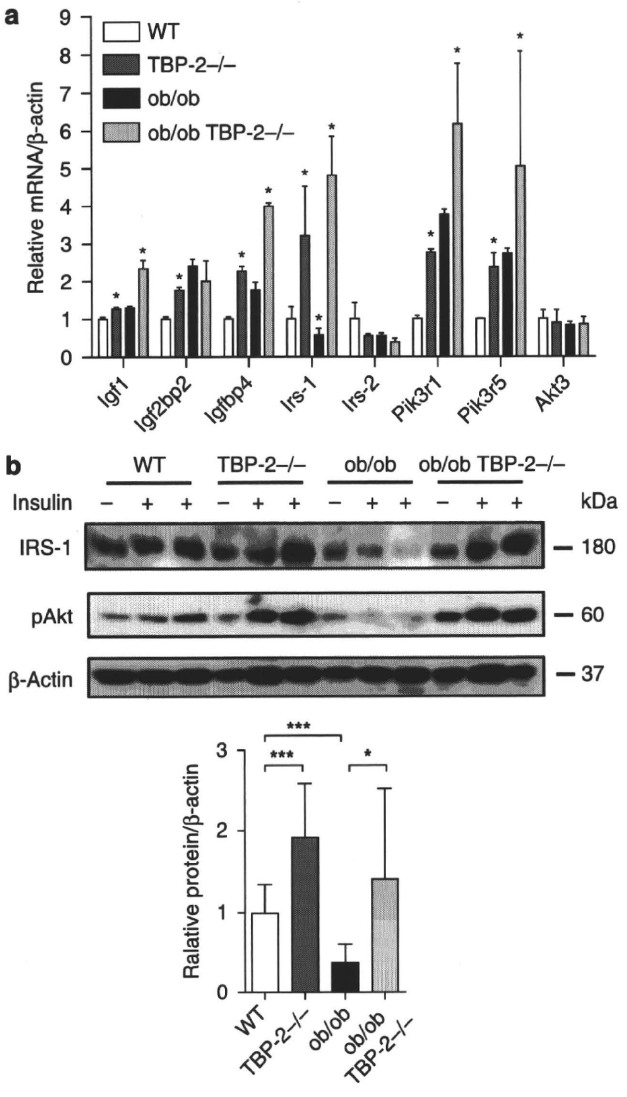

Figure 3 | Insulin signalling-related genes are upregulated by TBP-2 deficiency in skeletal muscle. The expression of insulin signal-related genes from the skeletal muscle of 10 weeks aged WT (white bar), TBP-2−/− (dark grey bar), ob/ob (black bar) and ob/ob·TBP-2−/− (light grey bar) mice. (**a**) Real-time PCR analyses were performed. Asterisk indicates $*P<0.05$;WT versus TBP-2−/−, WT versus ob/ob, ob/ob versus ob/ob·TBP-2−/−. (**b**) Immuno blotting (IB) analyses, *n* per group 3–5 each. Two U kg^{-1} insulin (+) or saline (−) was injected. Densitometric quantification of IRS-1/β-actin is shown in the bar graph. Data are presented as mean±s.d. $*P<0.05$, $***P<0.001$, versus control (*t*-test).

was not affected by dox-off-dependent TBP-2 induction in β-cells (Fig. 5l). Furthermore, effects of TBP-2 on insulin secretion stimulated by fuel secretagogues, which bypass glycolysis and are metabolized in mitochondria to generate ATP, were determined using methods previously described[32]. Insulin secretion induced by pyruvate and α-ketoisocaprotate plus monomethyl succinate was also suppressed by TBP-2 overexpression in β-cells (Fig. 5m). These results indicate that impaired GSIS by TBP-2 induction is attributable to reduction in mitochondrial metabolism, but not to a decrease in glycolysis.

TBP-2 has been reported to enhance apoptosis in pancreatic β-cells and other cells[21]. TBP-2 induction did not increase apoptosis in 48 h, but apoptosis was slightly increased on 72 h after high (20 mM) glucose treatment (Fig. 5n). β-Cell apoptosis was not changed significantly between ob/ob and ob/ob TBP-2−/− mice generated in a C57BL/6J background at 10 weeks of age (Supplementary Figs S3a,b and S4a), whereas TBP-2 deficiency suppressed β-cell apoptosis at age 36 weeks in C57BL/6J background mice (Supplementary Fig. S4b,c).These results suggest that TBP-2 negatively regulates GSIS by suppressing glucose-induced mitochondrial ATP production in INS-1 cells and islets before causing apoptosis. Treatment with reactive oxygen species scavengers (vitamins C+E) scarcely recovered the insulin secretion suppressed by TBP-2 overexpression in INS-1 cells (Supplementary Fig. S5), suggesting that mitochondrial dysfunction caused by TBP-2 is not mainly attributed to an increase in reactive oxygen species by reducing the scavenger effect of thioredoxin.

TBP-2 enhances UCP-2 transcriptional activity. Impairment in mitochondria ATP production often occurs with uncoupling[24]. Mitochondrial UCP-2 is a key regulator of ATP production and insulin secretion in pancreatic β-cells, and UCP-2 deficiency has been shown to improve GSIS and glucose-induced ATP production in ob/ob mice[24]. Thus, we measured UCP-2 mRNA in TBP-2-overexpressed INS-1 cells. Strikingly, there was a significant increase in UCP-2 mRNA levels in the TBP-2-induced cells (Fig. 6a). Furthermore, TBP-2 induction also increased UCP-2 protein levels in the mitochondria of INS-1 cells (Fig. 6b). UCP-2 expression is known to be upregulated by the increase in activity of transcriptional co-activators; e.g., PPARγ co-activator-1α (PGC-1α)[33]. TBP-2 is also induced by PGC-1α overexpression in INS-1 cells (Fig. 6c). We examined the effect of TBP-2 overexpression on activity of UCP-2 -86 promoter, containing Sp1, SRE and double E-box elements, the essential elements for a response to fatty acids and PGC-1α[33,34]. TBP-2 enhanced UCP-2 transcriptional activity through this -86 promoter region and the PGC-1α-induced activation was also augmented by TBP-2 expression (Fig. 6d), suggesting that TBP-2 enhances UCP-2 transcriptional activity and expression in INS-1 cells. To investigate how TBP-2 regulates UCP-2 transcriptional activity, we tested whether TBP-2 affects PGC-1α protein levels. Dox-off-dependent TBP-2 overexpression did not change PGC-1α protein levels (Supplementary Fig. S6). Next, we used chromatin immunoprecipitations (ChIPs) to investigate whether TBP-2 expression influences PGC-1α binding efficiency to the UCP-2 promoter region. Sheared chromatin was collected from INS-1 cells treated with or without doxycycline, and then immunoprecipitated with anti-RNA polymerase II or control-mouse immunoglobulin G or anti-PGC-1α antibody. PCR was performed with primers flanking the SP1, SRE and E-boxes region of UCP-2 (UCP-2 -86). PGC-1α was recruited to the UCP-2 -86 promoter region and dox-off-dependent TBP-2 overexpression enhanced PGC-1α binding efficiency to the region (Fig. 6e,f). These results indicate that TBP-2 facilitates PGC-1α recruitment in the UCP-2 promoter region, enhancing UCP-2 transcriptional activity in INS-1 cells. Next, we tested whether TBP-2-dependent UCP-2 expression is critical for aggravated GSIS using UCP-2 knockdown in dox-off-dependent TBP-2-overexpressing INS-1 cells. UCP-2 knockdown reversed suppression of GSIS by TBP-2 induction (Fig. 6g and Supplementary Fig. S7), suggesting that TBP-2-induced suppression of GSIS is mainly through UCP-2 expression. Furthermore, the expression level of UCP-2 mRNA was enhanced in islets of ob/ob mice, whereas TBP-2 deficiency dramatically reduced it in ob/ob islets (Fig 6h). Mitochondrial mass, determined as mitochondrial coding gene (mtDNA)/nuclear coding gene (COX I) expression ratio in pancreatic islets, was not affected by TBP-2 deficiency (Fig. 6i). Next, we examined the effect of the mitochondrial uncoupler carbonyl cyanide m-chlorophenyl-hydrazone (cccp) on GSIS in Tet-TBP-2 INS-1 cells with or without doxycycline and in TBP-2 deficient ob/ob islets. Uncoupling by cccp decreased the GSIS at the concentration 25–1,000 nM (Supplementary Fig. S8a). This result suggests that mitochondria metabolism is responsible for GSIS in β-cells and is tightly regulated by uncoupling. In dox-off tet-TBP-2 INS-1 cells, TBP-2 overexpression suppressed the GSIS equivalent

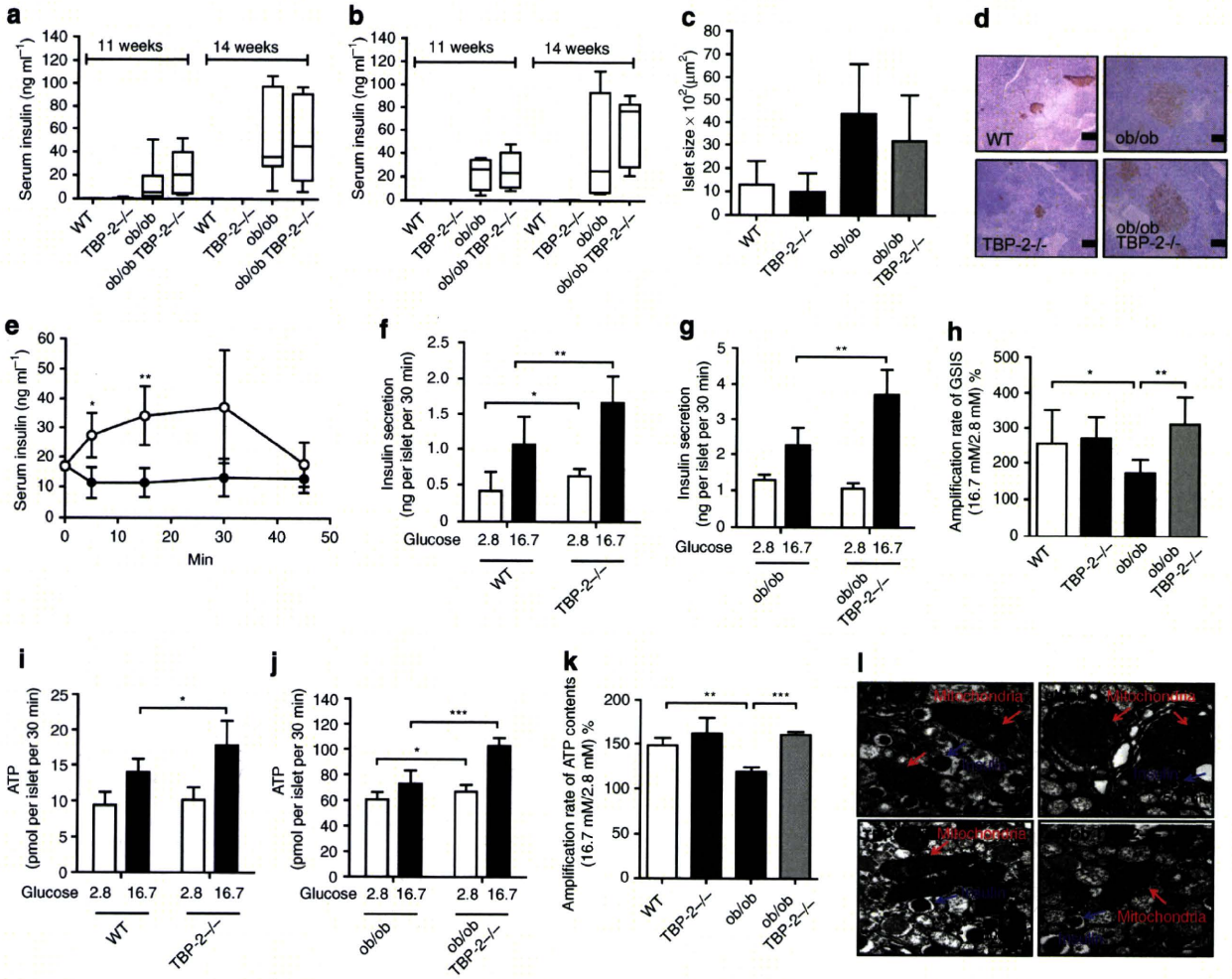

Figure 4 | Impairment of glucose-stimulated insulin secretion in ob/ob mice is improved by TBP-2 deficiency *in vivo* and *ex vivo*. Serum insulin concentrations at 11 and 14 weeks aged male (**a**) and female (**b**) mice. The median lines are shown in box graphs. $n = 6$–12 per group. Physiological analyses of islet mass (**c**) and insulin immunostaining of islets (**d**) in 10 weeks aged mice. Scale bars, 100 μm; $n = 3$ per group. (**e**) Serum insulin levels during intraperitoneal glucose tolerance tests (IPGTTs). Following an overnight fast, mice were injected with 1 g kg^{-1} glucose, IP (time 0). Serum insulin values were assessed before and at 5, 15, 30 and 45 min into the IPGTT. ob/ob (closed circle, $n = 6$), ob/ob·TBP-2−/− (open circle, $n = 5$). (**f**–**k**) Batches of 10 pancreatic islets isolated from WT, TBP-2−/−, ob/ob and ob/ob·TBP-2−/− mice of 10 weeks age were stimulated with 2.8 mM (open bar) or 16.7 mM glucose (closed bar) for 30 min. Insulin secretion (**f**–**h**) and ATP contents (**i**–**k**) were measured by radioimmunoassay and a luminometer, respectively. WT was compared with TBP-2−/− (**f**, **i**) or ob/ob with ob/ob·TBP-2−/− (**g**, **j**). Amplification rate of insulin secretion (**h**) and ATP contents (**k**) at high (16.7 mM) glucose compared with basal (2.8 mM) glucose stimulation for 30 min. (**l**) Electron microscopic images of islet sections (×30200; scale bar, 500 nm). Magnified areas of individual β-cell mitochondria. Red arrows highlight individual mitochondria and blue arrows highlight insulin granules. *Swelling and disappearance of cristae structures of mitochondria. Data are presented as mean±s.d. *$P < 0.05$, **$P < 0.01$, ***$P < 0.001$, versus control (*t*-test).

to the level elicited by 25 nM cccp (Supplementary Fig. S8b). More importantly, cccp had a larger effect on GSIS and glucose-induced ATP production in TBP-2-deficient ob/ob islets compared with ob/ob islets (Fig. 6j,k). These results suggest that TBP-2-dependent regulation of GSIS is mainly achieved through mitochondrial uncoupling and metabolism.

These results suggest that TBP-2 does not affect mitochondrial biogenesis but enhances UCP-2 transcriptional activity through the PGC-1α-dependent pathway, and the induction of the TBP-2-UCP-2 axis causes the defect of GSIS in ob/ob mice.

Mybbp1a is a novel candidate binding protein for TBP-2. To obtain further insight on how TBP-2 regulates gene expression in β-cells, we purified the TBP-2 protein complex using tosyl (p-toluene sulfonyl)-activated magnetic beads (Ts beads). His-tagged-TBP-2 protein was conjugated to the beads and incubated with nuclear extract of INS-1 cells. After washing, the eluate fractions were subjected to SDS gel electrophoresis and silver staining (Fig. 7a). The specific bands on silver staining were subjected to proteolytic digestion and mass spectrometry. Mybbp1a (p160), Mybbp1a (p140), GCN and NonO/p54nrb homologue were identified (Fig. 7b and Supplementary Table S3). Intriguingly, Mybbp1a is reported to inhibit PGC-1α function and transcription of PGC-1α target genes[35]. Therefore, we examined the interaction between TBP-2 and Mybbp1a. We showed that Mybbp1a is detected in elution samples from TBP-2 protein beads by anti-Mybbp1a antibody (Fig. 7c). To determine whether TBP-2 and Mybbp1a interact directly *in vivo*, we performed co-immunoprecipitation using FLAG-HA-tagged Mybbp1a and Myc-tagged TBP-2 expression vectors. Myc-tagged TBP-2 was co-immunoprecipitated with FLAG-HA-tagged Mybbp1a in HEK293 cells (Fig. 7d). Finally, we examined whether Mybbp1a regulates UCP-2 transcriptional activity. Mybbp1a suppressed PGC-1α-dependent UCP-2 transcriptional activity and the suppression was reversed by TBP-2

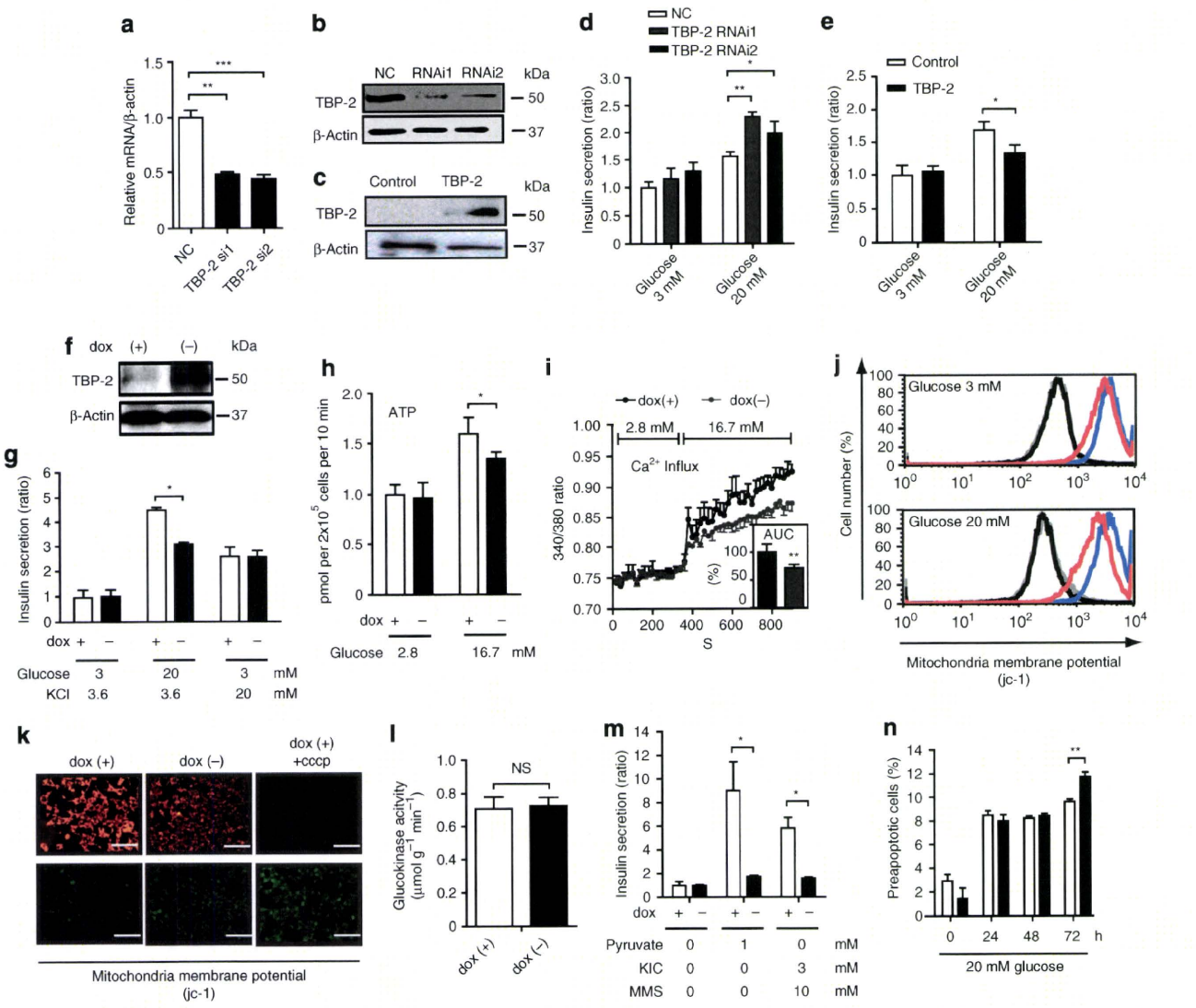

Figure 5 | TBP-2 suppresses glucose-induced mitochondrial energy production and insulin secretion in β-cells. Transient TBP-2 knockdown by TBP-2 siRNA (RNAi1 and RNAi2) and negative control siRNA (NC) in INS-1 cells. The expression of TBP-2 was determined by qRT–PCR (**a**) at 48 h after transfection and by immunoblot analysis (**b**) at 72 h after transfection. (**c**) Transient TBP-2 overexpression in INS-1 cells after 24 h. The expression of TBP-2 was determined by immunoblot analyses. Augmentation or suppression of GSIS in TBP-2 knockdown (**d**) or TBP-2 overexpression (**e**) cells in RPMI cultured medium. Statistic insulin secretion assays were analysed in INS-1 cells. (**f**) Construction of the doxycycline (dox)-off-dependent TBP-2-overexpressed INS-1 cells. TBP-2 protein was suppressed by 1000 ng ml^{-1} dox and induced by dox removal. Cells were cultured with (+, open bar) or without (−, closed bar) dox for 24 h. INS-1 cells were incubated at low (2.8 or 3 mM) or high (16.7 or 20 mM) glucose and experiments were performed. Suppression of high (20 mM) GSIS (**g**), high (16.7 mM) glucose-enhanced ATP contents (**h**) and intracellular Ca^{2+} influx (**i**) by dox-off TBP-2 overexpression, but not KCl-induced insulin secretion (**g**). The inset bar graph shows area under the curve levels (%) of intracellular Ca^{2+} levels between 320 and 900 s (**i**). Decrease of mitochondrial membrane potentials (MMP) in dox-off TBP-2 overexpression in INS-1 cells. MMP of cultured cells in medium containing 3 mM (upper panel) or 20 mM (lower panel) glucose for 24 h was analysed by flow cytometry (**j**) or in cultured medium by fluorescence microscopy (**k**) using jc-1 reagent, scale bar is 100 μm. For disruption of MMP, 5 μM carbonyl cyanide m-chlorophenlhydrazone (cccp) reagent was used. Flow cytometer, blue; dox (+), red; dox (−), black; dox (+) + cccp, grey; dox (−) + cccp. (**l**) Glucokinase (GK) activities in INS-1 cells, NS, nonsignificant. (**m**) Suppression of pyruvate (sodium pyruvate) or 2-ketoisohexanoic acid (KIC) and methylsaccinic acid (monomethyl succinate)-stimulated insulin secretion by dox-off-dependent TBP-2 overexpression. (**n**) A flow cytometric analyses with Annexin V-fluorescein isothiocyanate and propidium iodide staining in the dox-off TBP-2-overexpressed INS-1 cells. Preapoptotic cells were calculated from triplicate samples (%). Data are presented as mean±s.d. *P<0.05, **P<0.01, ***P<0.001, versus control (t-test).

co-expression (Fig. 7e). These results provide a model that TBP-2 suppresses Mybbp1a function possibly through protein–protein interaction, leading to the activation of PGC-1α-dependent UCP-2 transcription (Fig. 7f).

Discussion

In this study, we demonstrated that disruption of TBP-2 expression augments both insulin sensitivity and secretion, resulting in the amelioration of glucose intolerance in a diabetic mice model where TBP-2 expression is increased. The mechanism by which TBP-2 is increased in several tissues and pancreatic islets of ob/ob mice is presently unknown. It is possible that high blood glucose or obese-induced adipocytokines enhance TBP-2 expression, as TBP-2 is upregulated by several stimulations and stresses[36,37]. Several reports have shown that TBP-2 expression is regulated by mitochondrial metabolism and glycolysis through the transcription factor

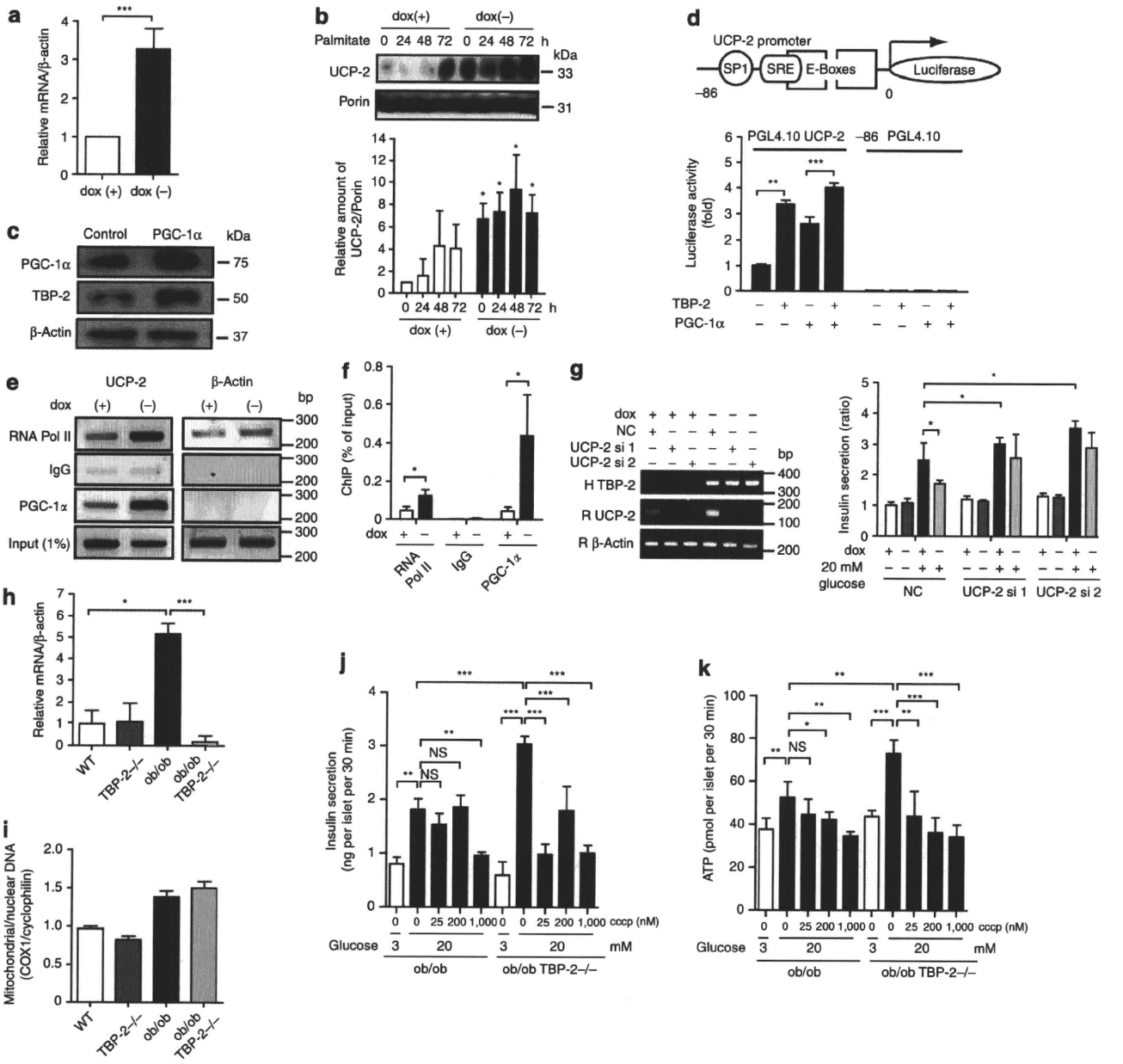

Figure 6 | TBP-2 enhances UCP-2 transcriptional activity. (**a**) Quantitative RT–PCR (qRT–PCR) analyses of UCP-2 mRNA expression in dox-off-dependent TBP-2-overexpressed INS-1 cells with or without dox. (**b**) Immuno blotting to determine UCP-2 expression in mitochondria in dox-off TBP-2 overexpression in INS-1 cells with or without palmitate (300 μM) for the indicated time. Densitometric quantification of the UCP-2/Porin ratio in mitochondria of INS-1 cells is shown in a bar graph. (**c**) Immuno blotting analyses to detect expression of PGC-1α, TBP-2 and β-actin in INS-1 cells, transiently transfected with PGC-1α plasmid for 24 h. (**d**) INS-1 cells were transfected with PGL4.10 UCP-2 -86 or PGL4.10-luciferase reporter plasmid and each expression plasmid for PGC-1α and TBP-2, as indicated. Luciferase reporter activity was normalized by *Renilla* luciferase activity. (**e**) ChIP assay of PGC-1α protein binding to endogenous *UCP-2* promoter. Chromatin extracts from INS-1 cells in dox-off-dependent TBP-2-overexpressed INS-1 cells with or without dox were precipitated in the presence of control-mouse IgG, anti-RNA polymerase II (RNA pol II) or anti-PGC-1α antibody. Primers for PCR are rat *UCP-2* promoter region primers and rat *β-actin* primers. (**f**) qRT–PCR analyses for ChIP were performed. (**g**) Insulin secretion in dox-off-dependent TBP-2 overexpressing INS-1 cells with or without dox and knockdown of UCP-2 (si1 and si2). The left panel shows RT–PCR analysis of human *TBP-2* expression (H TBP-2) to confirm the effect of dox, rat *UCP-2* expression (R UCP-2) to confirm the knockdown effect, and rat *β-actin* (R β-actin). (**h**) qRT–PCR analyses of UCP-2 mRNA in isolated pancreatic islets of WT, TBP-2−/−, ob/ob and ob/ob·TBP-2−/− mice. (**i**) qRT–PCR was used to determine mitochondria content by measuring the expression of mitochondrial gene (COX I)/nuclear gene (cyclophilin) ratios. (**j**, **k**) Effect of cccp treatment for 30 min on insulin secretion (**j**, ng per islet per 30 min) and ATP levels (**k**, pmol per islet per 30 min) in ob/ob and ob/ob TBP-2−/− islets. Data are presented as mean±s.d. $^{*}P<0.05$, $^{**}P<0.01$, $^{***}P<0.001$, versus control (*t*-test).

MondoA[38–41]. These reports indicate that TBP-2 expression is tightly regulated in response to changes in energy status.

TBP-2 deficiency in ob/ob mice improved hyperglycaemia, glucose intolerance and insulin resistance without amelioration of obesity (Fig. 1e–m). A previous study showed that HcB-19 mice crossed with ob/ob mice improved glucose tolerance[21]. Other studies showed that silencing of TBP-2 expression enhanced glucose uptake in adipocytes and human skeletal myocytes, whereas TBP-2 overexpression

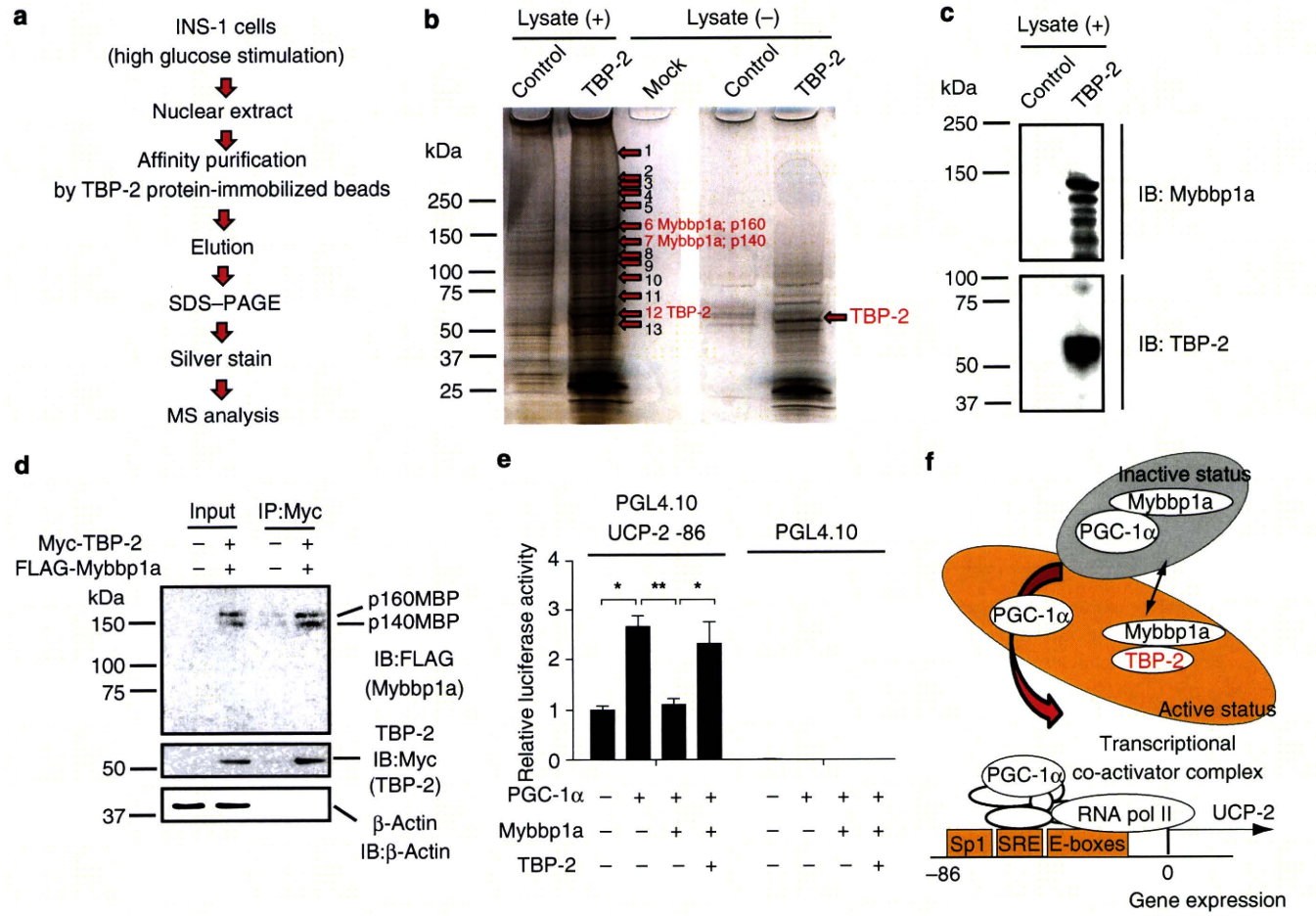

Figure 7 | Mybbp1a was identified as a novel candidate binding protein for TBP-2. (**a**) Purification scheme for the TBP-2 containing protein complex in β-cell nuclear extracts. TBP-2 binding proteins were purified from INS-1 nuclear extracts by using TBP-2 protein-immobilized (TBP-2) or control beads. (**b**) Identification of the TBP-2 complex. Silver staining was performed. Numbers indicate individual candidate proteins interacting with TBP-2. (**c**) Eluted proteins were analysed by immuno blotting (IB) for Mybbp1a and TBP-2 antibody. (**d**) Co-immunoprecipitation analyses. Input (left, 5% lysate) and anti-Myc immunoprecipitates (right, IP:Myc) from HEK293 cells transfected with pCMV-tag2A and pCMV-tag3B vector (−) or FLAG-HA-Mybbp1a and Myc-TBP-2 vector (+) were analysed by immunoblotting (IB) with antibodies to FLAG, Myc and β-actin. The positions for Mybbp1a (p160; p160MBP) and Mybbp1a (p140; p140MBP) (upper), TBP-2 (middle) and β-actin (lower) are shown. (**e**) Luciferase activity of the UCP-2 -86 enhancer region. INS-1 cells were transfected with PGL4.10 UCP-2 -86 or PGL4.10-luciferase reporter plasmid and each expression plasmid for PGC-1α, Mybbp1a and TBP-2, as indicated. Luciferase reporter activity was normalized by *Renilla* luciferase activity. (**f**) A schematic model of TBP-2 function in β-cells. Mybbp1a binds PGC-1α (inactive form) and inhibits UCP-2 transcriptional activity. Induced TBP-2 interacts with Mybbp1a and releases PGC-1α from Mybbp1a, facilitating PGC-1α recruitment on the UCP-2 promoter region. Data are presented as mean±s.d. $*P<0.05$, $**P<0.01$, versus control (*t*-test).

inhibited glucose uptake[19]. Entire or muscle-specific TBP-2−/− mice showed enhanced glucose uptake in the skeletal muscle and adipose with a high-fat diet[23,42]. The current study is consistent with these previous reports. The restoration of glucose tolerance in ob/ob·TBP-2−/− mice could not be explained by changes in energy balance or hormonal level of adipocytokines, such as adiponectin, free fatty acids and MCP-1. Insulin resistance in skeletal muscle and liver is mainly caused by inactivation of insulin/Akt signalling[1]. We showed that TBP-2 deficiency in ob/ob mice improved Akt signalling in muscle but not liver (Fig. 2k–p). Moreover, *IRS-1* gene and several insulin signalling genes were upregulated in skeletal muscle by TBP-2 deficiency both in WT and ob/ob mice (Fig. 3a and Supplementary Table S2). IRS-1 protein levels were downregulated in the skeletal muscle of ob/ob mice compared with that of WT mice, while IRS-1 protein levels were also upregulated by TBP-2 deficiency in both WT and ob/ob mice (Fig. 3b). As IRS-1 has a pivotal role in insulin sensitivity in muscle[27], TBP-2 regulates insulin signalling possibly through the regulation of *IRS-1* gene expression in muscle. Interestingly, TBP-2 deficiency did not change *IRS-2* gene expression, which is known as a main regulator of liver insulin sensitivity[43] in skeletal muscle (Fig. 3a). These results suggest that TBP-2 regulates IRS-1-related insulin sensitivity in skeletal muscle, but not IRS-2-related insulin sensitivity in liver. The molecular mechanism of how TBP-2 regulates the expression of IRS-1 and insulin signalling genes in skeletal muscle is now under investigation. We also found that gene expression of PPARs and their target genes, such as *PPARγ*, *PPARα*, *Acaca*, *Fabp3*, *Scd1* and *Pdk4*, are enhanced by TBP-2 deficiency in skeletal muscle (Supplementary Fig. S2), similar to previous reports in the liver and adipose tissue of TBP-2−/− mice[16,42]. As PPAR signalling augments insulin sensitivity[44], it may also be involved in enhanced insulin sensitivity by TBP-2 deficiency.

The GSIS was significantly impaired in ob/ob islets, whereas insulin secretion from ob/ob·TBP-2−/− islets was restored *in vivo* and *ex vivo*, suggesting that the ablation of TBP-2 in pancreatic islets of ob/ob mice augments GSIS. Our results indicate that upregulation of TBP-2 suppresses GSIS by reducing ATP production in pancreatic β-cells. Meanwhile, glycolytic activity was not changed by TBP-2 overexpression (Fig. 5l) in β-cell lines. Recently, several groups have

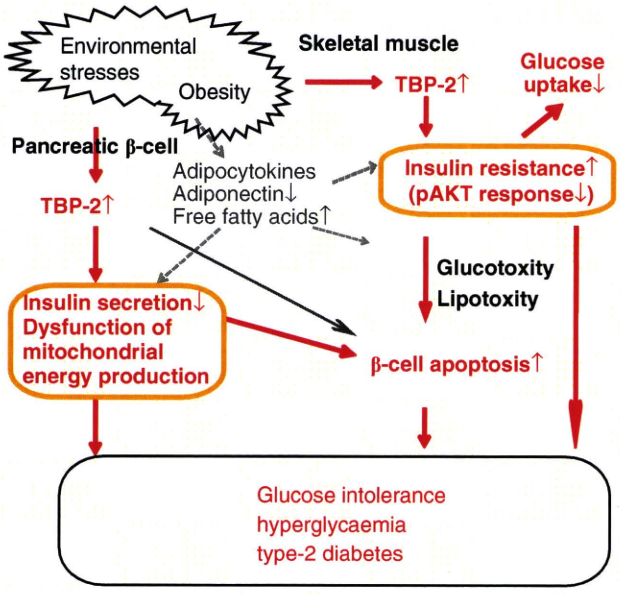

Figure 8 | A model for metabolic function of TBP-2 in diabetes. Role of TBP-2 in promoting obesity-induced type 2 diabetes. Environmental stresses including obesity cause upregulation of TBP-2. Sustained expression of TBP-2 may impair mitochondrial function and insulin secretion in β-cells and aggravate insulin resistance in skeletal muscle. Augmented expression of TBP-2 may also result in β-cell apoptosis. These changes lead to glucose intolerance and hyperglycaemia and obese-induced type 2 diabetes.

shown that TBP-2 regulates β-cell mass and β-cell apoptosis in C3H/He background mice and INS-1 cells[21,22,45,46]. Our results also support these previous studies. TBP-2 deficiency suppressed β-cell apoptosis at age 36 weeks in C57BL/6J background mice (Supplementary Fig. S4b,c). In contrast, while β-cell apoptosis was not changed significantly between ob/ob and ob/ob·TBP-2−/− mice generated in C57BL/6J background mice at 10 weeks age (Supplementary Figs S3a,b and S4a,c), TBP-2 deficiency improved GSIS in ob/ob mice at age 10–14 weeks. Taken together, improvement of GSIS by TBP-2 depletion *in vivo* was attributable to functional amelioration of β-cells but not to an increase in β-cell mass, at least, in mice of this age. Moreover, impaired GSIS without reduction in β-cell mass preceded significant detection of apoptosis in islets in ob/ob mice, which supports the pathogenic importance of functional impairment of β-cells. Thus, TBP-2 seems to regulate not only β-cell apoptosis but also β-cell energy metabolism in the diabetic condition.

Impairment of GSIS in ob/ob mice was improved by TBP-2 deficiency. This phenotype resembles ob/ob mice lacking UCP-2, which is a negative regulator of GSIS[24]. We showed that TBP-2 deficiency cancelled upregulation of UCP-2 gene expression in ob/ob islets (Fig. 6h). Therefore, UCP-2 regulation by TBP-2 seems to be important in the development of the diabetic phenotype in ob/ob mice. UCP-2 knockdown recovered the TBP-2-dependent impairment in GSIS (Fig 6g). Furthermore, the mitochondrial uncoupling reagent cccp had a greater effect on GSIS and glucose-induced ATP production in TBP-2-deficient ob/ob islets compared with those in ob/ob islets (Fig. 6j,k). These results suggest that TBP-2-dependent regulation of GSIS is mainly due to mitochondrial uncoupling derived from UCP-2 expression.

The results from a ChIP assay indicated that TBP-2 regulates UCP-2 expression by facilitating PGC-1α recruitment to the UCP-2 promoter region. Furthermore, we identified Mybbp1a as a novel binding protein of TBP-2. Mybbp1a is reported to inhibit PGC-1α function and transcription of PGC-1α target genes through direct protein–protein interaction[35]. Indeed, Mybbp1a overexpression suppressed PGC-1α-dependent UCP-2 transcriptional activity (Fig. 7e), and TBP-2 overexpression hampered the effect of Mybbp1a on PGC-1α-dependent UCP-2 promoter activity in INS-1 cells (Fig. 7e). These results suggest a model that TBP-2 regulates UCP-2 expression through Mybbp1a and PGC-1α pathway (Fig. 7f). Recently, it has been reported that α-arrestin family proteins are considered to act as adaptor protein for the E3-ubiquitin ligases in the yeast system[47] and TBP-2 interacts with WW domain of HECT domain containing E3-ubiquitin ligases through the PPxY motif of TBP-2[12]. These reports provide a hypothesis that TBP-2 negatively regulates Mybbp1a by protein degradation through E3-ubiquitin ligases. This possibility should be further investigated.

In this study, we demonstrated that ablation of TBP-2 expression augments both insulin sensitivities by enhancing IRS-1/Akt signalling in skeletal muscle and GSIS by suppressing UCP-2 transcription and maintaining mitochondrial function in pancreatic β-cells, resulting in the amelioration of glucose intolerance and hyperglycaemia. The proposed mechanism for this effect is summarized in Figure 8 and Supplementary Figure S9. These findings raise the possibility that the inhibition of either TBP-2 activity or expression may be a novel therapeutic approach for type 2 diabetes.

Methods

Animal experiments. TBP-2-knockout mice were generated as described previously[17]. Mice were backcrossed for at least 11 generations with a C57B/6 genetic background. Animals were maintained in a specific pathogen-free animal facility on a 12-h light–dark cycle at an ambient temperature of 21 °C. They were given free access to water and food.

Age- and sex-matched mice were used for all animal experiments. All procedures involving animals were performed in accordance with protocols approved by the Animal Care and Research Advisory Committee of the Institute for Virus Research at Kyoto University.

Generation of TBP-2-deficient ob/ob mice. C57BL6 ob/+ were purchased from the Jackson Laboratory. To generate ob/ob·TBP-2−/− mice, TBP-2−/− mice were crossed with ob/+ mice creating compound heterozygotes, ob/OB·TBP-2+/−. In the second cross, compound heterozygotes were crossed to generate the following animals of which both males and females were collected and studied further: WT mice (+/+ at both ob and TBP-2 loci), ob/ob mice (ob/ob at the ob locus and +/+ at the TBP-2 locus), TBP-2−/− mice (+/+ at the ob locus and −/− at the TBP-2 locus) and ob/ob·TBP-2−/− mice (ob/ob at the ob locus and −/− at the TBP-2 locus). The ob allele was genotyped as previously described[48].

Intraperitoneal glucose or ITTs. For the intraperitoneal (IP) glucose tolerance test, following an overnight fast, ob/ob and ob/ob·TBP-2−/− mice were injected with 0.5 g kg^{-1} or 1 g kg^{-1} glucose. Blood glucose values were assessed before and at 15, 30, 60 and 120 min after the IP administration of glucose using glucose PILOT. Serum insulin values were assessed before and at 5, 15, 30 and 45 min after the IP administration of glucose using an Insulin ELISA kit. For the IP ITTs, mice were fasted for 6 h and then injected with 1 U kg^{-1} insulin.

Cell culture and transfection. INS-1 cells were cultured at 37 °C with 5% CO_2 in air in RPMI1640 (Sigma-Aldrich), supplemented with 10% (v/v) fetal bovine serum, 1% (v/v) penicillin/streptomycin antibiotics, 10 mM HEPES, 2 mM L-glutamine, 1 mM sodium pyruvate and 50 μM β-mercaptoethanol (RPMI for INS-1 medium). INS-1 cells were transfected with TBP-2 small interfering RNA (siRNA) or negative control siRNA (Qiagen) for 72 h or with pCMV-Tag2B-TBP-2 or control pCMV-Tag2B (Stratagene) plasmid for 24 h and cultured with RPMI1640 for INS-1 medium.

Isolated pancreatic islet studies. Pancreatic islets were isolated from mice according to a method used for rats[49].

Generation of INS-1 cells with inducible TBP-2 expression. Stable INS-1 cells, which carry the reverse tetracycline/doxycycline-dependent transactivator pTRE2 (pTet-Off, Clontech), were prepared. After selection with 500 μg ml^{-1} G418, resistant colonies were isolated with limiting dilution methods in 96-well plates. One clonal line that exhibited very high tetracycline-off-inducible luciferase activity and undetectable basal luciferase activity was chosen and used for a second round of transfection with the TBP-2 expression plasmid (pTRE2 pur-TBP-2-FLAG). After selection with 500 ng ml^{-1} puromycin and doxycycline-off-induced TBP-2 expression, clones were isolated.

Insulin secretion assay using INS-1 cells. INS-1 cells were transfected with TBP-2 siRNA (Rn_Txnip_1 and 5) or UCP-2 siRNA (Rn_UCP-2_5 and 6) or negative control siRNA (purchased from Qiagen) for 72 h, or with pCMV-Tag2A-TBP-2 or

control pCMV-Tag2A (Stratagene) plasmid for 24 h. Then, the cells were cultured in Krebs Ringer bicarbonate buffer (KRBB) (as mentioned below) or RPMI1640 for INS-1 medium with 2.8 mM (5 mM) or 16.7 mM (20 mM) glucose containing RPMI medium and the supernatant was collected 30 min after the addition of glucose. Insulin concentration was measured by an Insulin ELISA kit. Similar analyses were performed in Tet-TBP-2 INS-1 cells pretreated with or without doxycycline for 24 to 48 h. One mM pyruvate (sodium pyruvate, Nacalai Tesque) or 3 mM α-ketoisocaprotate (2-ketoisohexanoic acid, Nacalai Tesque) and 10 mM monomethyl succinate (methylsuccinic acid sodium salt, Sigma-Aldrich)-stimulated insulin secretion assays were performed in Tet-TBP-2 INS-1 cells.

Insulin secretion assay using primary mouse pancreatic islet. Insulin release from intact islets was monitored using batch incubation methods[50]. Isolated pancreatic islets were precultured at 37 °C for 30 min with gentle swinging (50 times per min) in KRBB containing 129.4 mM NaCl, 3.7 mM KCl, 2.7 mM $CaCl_2$, 1.3 mM KH_2PO_4, 1.3 mM $MgSO_4$, 24.8 mM $NaHCO_3$ (equilibrated with 5% CO_2, 95% O_2, pH 7.4), and 0.2 % (vol/vol) bovine serum albumin (fraction V) with 2.8 mM glucose. Next, the pancreatic islets were incubated for 30 min in KRBB buffer with glucose 2.8 or 16.7 mM to determine insulin secretion levels. At the end of the incubation period, islets were pelleted by centrifugation, and aliquots of the buffer were sampled. The amount of immunoreactive insulin was determined by radioimmunoassay, using rat insulin as standard.

ATP contents assay. INS-1 cells (2.0×10^5 cells per 24-well plate) or isolated pancreatic islets were precultured in KRBB buffer with 2.8 mM glucose for 2 h or 30 min, and were batch incubated for 10 or 30 min in KRBB with 2.8 or 16.7 mM glucose, respectively. After immediate addition of $HClO_4$, cells were sonicated in ice-cold water for 10 min, and centrifuged. Part of the supernatant fraction was mixed with HEPES and Na_2CO_3 and the ATP content in the cells was determined by luminometer as previously described[50].

Intracellular Ca^{2+} assay. INS-1 cells were precultured for 2 h in KRBB with 2.8 mM glucose and then cells were loaded with 5μM Fura-PE3 AM in KRBB containing 2.8 mM glucose and 0.2% bovine serum albumin at 37 °C for 20 min. Intracellular Ca^{2+} concentration was measured by the ratio of emission fluorescence of 510 nm by excitation at 340 and 380 nm as previously described[50].

Measurement of mitochondrial membrane potentials. Briefly, INS-1 cells were preincubated in KRBB with 3 and 20 mM glucose or in cultured medium for 24 h, and the cells were resuspended in 0.5 ml of ice-cold PBS, then cultured with 10 nM jc-1 (Sigma-Aldrich, J-4519) for 15 min in 5% CO_2 at 37 °C with or without 5 μM cccp, a protonophore that completely dissipated $\Delta\psi$, and was analysed by flow cytometry (FACSCanto II, BD Bioscience) or fluorescence microscopy (Biozero, Keyence). The greater the mitochondrial membrane potential, the more jc-1 aggregates form that have a red fluorescent emission signal, as opposed to the jc-1 monomer that fluorescences green. Data acquisition and analysis were performed using Cell Quest Software.

Luciferase reporter assays. INS-1 cells were transiently transfected with pGL4.10 luc2 vectors containing UCP-2 -86 enhancer region (5′-GGCTCCGCCTCGT CACGCCACGCCCCGACCACGCCCTCTAGA-3′) or pGL4.10 luc2 vectors, with the pCMV-PGC-1α, pCMV-Tag2A-TBP-2 and FLAG-HA-p160 MBP plasmids. FLAG-HA-p160 MBP was kindly provided by Dr Shunsuke Ishii. As a control, the total amount of vectors for transfection was adjusted by the amount of the pCMV-Tag2A vector. After 18 h of transfection, luciferase activity was quantified using the luciferase assay system (Promega). pRL-TK (Promega) was used to monitor *Renilla* luciferase gene expression as a control for the efficiency of transfection.

Cell culture of primary MEFs. Primary MEFs were derived from 13.5-day-old embryos from TBP-2 +/− mice, and then the MEFs were genotyped to obtain TBP-2 −/− and TBP-2 +/+ MEFs. Cells were maintained in DMEM with 10% fetal calf serum, 1% penicillin and 0.5% L-glutamine. TBP-2 mRNA expression was confirmed by semiquantitative RT–PCR analysis. Primer sequences are listed in Supplementary Table S4.

Quantitative (semiquantitative) RT-PCR analysis. Total RNA was extracted from INS-1 cells or handpicked freshly isolated islets using TRIzol reagent (Invitrogen). Reverse transcription was performed with SuperScript III (Invitrogen) or PrimeScript RT (TAKARA). Real-time RT–PCR was performed using SYBR Premix Ex Tag II(TAKARA). The internal control used was β-actin. PCR analyses were carried out using the oligonucleotide primers listed in Supplementary Table S4.

Chromatin immunoprecipitation. Chromatin was prepared from Tet-TBP-2 INS-1 cells treated with or without doxycycline. Briefly, 5×10^6 cells were crosslinked with 1% formaldehyde for 10 min, followed by the addition of glycine at 125 mM. Chromatin was sheared by enzymes (CHIP IT Express Kit, Active Motif). Chromatin was immunoprecipitated with 2 μg anti-RNA polymerase II (Active Motif), control-mouse immunoglobulin G (Active Motif) or anti-PGC-1α antibodies (Santa Cruz). GATCTGAGACAGGGAGACTCTAGG and GGAGAATACACA GGAGAACACAGG primers were used to amplify the UCP-2 SP1, SRE, E-boxes region. Rat β-actin enhancer primers (Active Motif) were used as control. PCR was carried out with one cycle at 95 °C for 2 min; 36 cycles at 94 °C for 10 s, 60 °C for 30 s, 68 °C for 1 min; and one cycle at 68 °C for 5 min.

Co-immunoprecipitation. To investigate interactions between TBP-2 and Mybbp1a *in vivo*, Myc-TBP-2 and FLAG-HA-Mybbp1a or pCMV-tag3B and pCMV-tag2A (as control) were co-expressed in HEK293 cells. Cells were lysed in lysis buffer (CellLytic M Cell Lysis Reagent, Sigma-Aldrich), and insoluble materials were precipitated by centrifugation at 15,000 × *g* for 15 min. The resulting supernatants were incubated with anti-Myc agarose beads (MBL), and bound material was eluted with Myc-peptide (500 μg ml^{-1}, MBL). Protein–protein interaction was assessed by immunoblotting using anti-FLAG antibody (Sigma-Aldrich) or anti-Myc antibody (Sigma-Aldrich).

Statistical method. Results were expressed as the mean±s.d. Statistical comparisons were made using Student's *t*-test. A statistically significant difference was defined as $^*P<0.05$, $^{**}P<0.01$, $^{***}P<0.001$.

References

1. Biddinger, S. B. & Kahn, C. R. From mice to men: insights into the insulin resistance syndromes. *Annu. Rev. Physiol.* **68,** 123–158 (2006).
2. Guilherme, A., Virbasius, J. V., Puri, V. & Czech, M. P. Adipocyte dysfunctions linking obesity to insulin resistance and type 2 diabetes. *Nat. Rev. Mol. Cell Biol.* **9,** 367–377 (2008).
3. Pratley, R. E. & Weyer, C. The role of impaired early insulin secretion in the pathogenesis of Type II diabetes mellitus. *Diabetologia* **44,** 929–945 (2001).
4. Anello, M. *et al.* Functional and morphological alterations of mitochondria in pancreatic beta cells from type 2 diabetic patients. *Diabetologia* **48,** 282–289 (2005).
5. Maechler, P. & Wollheim, C. B. Mitochondrial function in normal and diabetic beta-cells. *Nature* **414,** 807–812 (2001).
6. Bodnar, J. S. *et al.* Positional cloning of the combined hyperlipidemia gene Hyplip1. *Nat. Genet.* **30,** 110–116 (2002).
7. Chen, K. S. & DeLuca, H. F. Isolation and characterization of a novel cDNA from HL-60 cells treated with 1,25-dihydroxyvitamin D-3. *Biochim. Biophys. Acta.* **1219,** 26–32 (1994).
8. Nishiyama, A. *et al.* Identification of thioredoxin-binding protein-2/vitamin D(3) up-regulated protein 1 as a negative regulator of thioredoxin function and expression. *J. Biol. Chem.* **274,** 21645–21650 (1999).
9. Nishinaka, Y. *et al.* Importin alpha1 (Rch1) mediates nuclear translocation of thioredoxin-binding protein-2/vitamin D(3)-up-regulated protein 1. *J. Biol. Chem.* **279,** 37559–37565 (2004).
10. Oka, S. *et al.* Thioredoxin-binding protein-2-like inducible membrane protein is a novel vitamin D3 and peroxisome proliferator-activated receptor (PPAR)gamma ligand target protein that regulates PPARgamma signaling. *Endocrinology* **147,** 733–743 (2006).
11. Patwari, P. *et al.* Thioredoxin-independent regulation of metabolism by the alpha-arrestin proteins. *J. Biol. Chem.* **284,** 24996–5003 (2009).
12. Zhang, P. *et al.* The ubiquitin ligase itch regulates apoptosis by targeting thioredoxin-interacting protein for ubiquitin-dependent degradation. *J. Biol. Chem.* **285,** 8869–79 (2010).
13. Zhou, R., Tardivel, A., Thorens, B., Choi, I. & Tschopp, J. Thioredoxin-interacting protein links oxidative stress to inflammasome activation. *Nat. Immunol.* **11,** 136–140 (2010).
14. Nishinaka, Y. *et al.* Loss of thioredoxin-binding protein-2/vitamin D3 up-regulated protein 1 in human T-cell leukemia virus type I-dependent T-cell transformation: implications for adult T-cell leukemia leukemogenesis. *Cancer Res.* **64,** 1287–1292 (2004).
15. Lee, K. N. *et al.* VDUP1 is required for the development of natural killer cells. *Immunity* **22,** 195–208 (2005).
16. Oka, S. *et al.* Thioredoxin binding protein-2/thioredoxin-interacting protein is a critical regulator of insulin secretion and peroxisome proliferator-activated receptor function. *Endocrinology* **150,** 1225–1234 (2009).
17. Oka, S. *et al.* Impaired fatty acid utilization in thioredoxin binding protein-2 (TBP-2)-deficient mice: a unique animal model of Reye syndrome. *FASEB J.* **20,** 121–123 (2006).
18. Hui, T. Y. *et al.* Mice lacking thioredoxin-interacting protein provide evidence linking cellular redox state to appropriate response to nutritional signals. *J. Biol. Chem.* **279,** 24387–24393 (2004).
19. Parikh, H. *et al.* TXNIP regulates peripheral glucose metabolism in humans. *PLoS Med.* **4,** e158 (2007).
20. Chutkow, W. A., Patwari, P., Yoshioka, J. & Lee, R. T. Thioredoxin-interacting protein (Txnip) is a critical regulator of hepatic glucose production. *J. Biol. Chem.* **283,** 2397–2406 (2008).
21. Chen, J. *et al.* Thioredoxin-interacting protein deficiency induces Akt/Bcl-xL signaling and pancreatic beta-cell mass and protects against diabetes. *FASEB J.* **22,** 3581–3594 (2008).
22. Chen, J., Saxena, G., Mungrue, I. N., Lusis, A. J. & Shalev, A. Thioredoxin-interacting protein: a critical link between glucose toxicity and beta-cell apoptosis. *Diabetes* **57,** 938–944 (2008).

23. Hui, S. T. *et al.* Txnip balances metabolic and growth signaling via PTEN disulfide reduction. *Proc. Natl Acad. Sci. USA* **105,** 3921–3926 (2008).
24. Zhang, C. Y. *et al.* Uncoupling protein-2 negatively regulates insulin secretion and is a major link between obesity, beta cell dysfunction, and type 2 diabetes. *Cell* **105,** 745–755 (2001).
25. Rosen, E. D. & Spiegelman, B. M. Adipocytes as regulators of energy balance and glucose homeostasis. *Nature* **444,** 847–853 (2006).
26. Sreekumar, R., Halvatsiotis, P., Schimke, J. C. & Nair, K. S. Gene expression profile in skeletal muscle of type 2 diabetes and the effect of insulin treatment. *Diabetes* **51,** 1913–1920 (2002).
27. Tamemoto, H. *et al.* Insulin resistance and growth retardation in mice lacking insulin receptor substrate-1. *Nature* **372,** 182–186 (1994).
28. Muoio, D. M. & Newgard, C. B. Mechanisms of disease: molecular and metabolic mechanisms of insulin resistance and beta-cell failure in type 2 diabetes. *Nat. Rev. Mol. Cell Biol.* **9,** 193–205 (2008).
29. Hackenbrock, C. R. Ultrastructural bases for metabolically linked mechanical activity in mitochondria. I. Reversible ultrastructural changes with change in metabolic steady state in isolated liver mitochondria. *J. Cell Biol.* **30,** 269–297 (1966).
30. Bonnard, C. *et al.* Mitochondrial dysfunction results from oxidative stress in the skeletal muscle of diet-induced insulin-resistant mice. *J. Clin. Invest.* **118,** 789–800 (2008).
31. Meglasson, M. D. & Matschinsky, F. M. Pancreatic islet glucose metabolism and regulation of insulin secretion. *Diabetes Metab. Rev.* **2,** 163–214 (1986).
32. MacDonald, M. J. Synergistic potent insulin release by combinations of weak secretagogues in pancreatic islets and INS-1 cells. *J. Biol. Chem.* **282,** 6043–6052 (2007).
33. Oberkofler, H., Klein, K., Felder, T. K., Krempler, F. & Patsch, W. Role of peroxisome proliferator-activated receptor-gamma coactivator-1alpha in the transcriptional regulation of the human uncoupling protein 2 gene in INS-1E cells. *Endocrinology* **147,** 966–976 (2006).
34. Medvedev, A. V. *et al.* Regulation of the uncoupling protein-2 gene in INS-1 beta-cells by oleic acid. *J. Biol. Chem.* **277,** 42639–42644 (2002).
35. Fan, M. *et al.* Suppression of mitochondrial respiration through recruitment of p160 myb binding protein to PGC-1alpha: modulation by p38 MAPK. *Genes Dev.* **18,** 278–289 (2004).
36. Ahsan, M. K., Nakamura, H., Masutani, H. & Yodoi, J. Thioredoxin and thioredoxin-binding protein-2 in cancer and metabolic syndrome. *Free Radic. Biol. Med.* **43,** 861–868 (2007).
37. Yoshihara, E., Chen, Z., Matsuo, Y., Masutani, H. & Yodoi, J. Thiol redox transitions by thioredoxin and thioredoxin-binding protein-2 in cell signaling. *Methods Enzymol.* **474,** 67–82 (2010).
38. Stoltzman, C. A. *et al.* Glucose sensing by MondoA:Mlx complexes: a role for hexokinases and direct regulation of thioredoxin-interacting protein expression. *Proc. Natl Acad. Sci. USA* **105,** 6912–6917 (2008).
39. Peterson, C. W., Stoltzman, C. A., Sighinolfi, M. P., Han, K. S. & Ayer, D. E. Glucose controls nuclear accumulation, promoter binding, and transcriptional activity of the MondoA-Mlx heterodimer. *Mol. Cell Biol.* **30,** 2887–2895 (2010).
40. Kaadige, M. R., Looper, R. E., Kamalanaadhan, S. & Ayer, D. E. Glutamine-dependent anapleurosis dictates glucose uptake and cell growth by regulating MondoA transcriptional activity. *Proc. Natl Acad. Sci. USA* **106,** 14878–14883 (2009).
41. Chen, J. L. *et al.* Lactic Acidosis Triggers Starvation Response with Paradoxical Induction of TXNIP through MondoA. *PLoS Genet.* **6,** e1001093 (2010).
42. Chutkow, W. A. *et al.* Deletion of the alpha-arrestin protein Txnip in mice promotes adiposity and adipogenesis while preserving insulin sensitivity. *Diabetes* **59,** 1424–1434 (2010).
43. Sesti, G. *et al.* Defects of the insulin receptor substrate (IRS) system in human metabolic disorders. *FASEB J.* **15,** 2099–2111 (2001).
44. Ferre, P. The biology of peroxisome proliferator-activated receptors: relationship with lipid metabolism and insulin sensitivity. *Diabetes* **53** (Suppl 1), S43–50 (2004).
45. Shaked, M. *et al.* Insulin counteracts glucotoxic effects by suppressing thioredoxin-interacting protein production in INS-1E beta cells and in Psammomys obesus pancreatic islets. *Diabetologia* **52,** 636–644 (2009).
46. Masson, E. *et al.* High beta-cell mass prevents streptozotocin-induced diabetes in thioredoxin-interacting protein-deficient mice. *Am. J. Physiol. Endocrinol. Metab.* **296,** E1251–1261 (2009).
47. Lin, C. H., MacGurn, J. A., Chu, T., Stefan, C. J. & Emr, S. D. Arrestin-related ubiquitin-ligase adaptors regulate endocytosis and protein turnover at the cell surface. *Cell* **135,** 714–725 (2008).
48. Hirasawa, T., Ohara, T. & Makino, S. Genetic typing of the mouse ob mutation by PCR and restriction enzyme analysis. *Exp. Anim.* **46,** 75–78 (1997).
49. Sutton, R., Peters, M., McShane, P., Gray, D. W. & Morris, P. J. Isolation of rat pancreatic islets by ductal injection of collagenase. *Transplantation* **42,** 689–691 (1986).
50. Fujimoto, S. *et al.* The novel insulinotropic mechanism of pimobendan: Direct enhancement of the exocytotic process of insulin secretory granules by increased Ca2+ sensitivity in beta-cells. *Endocrinology* **139,** 1133–1140 (1998).

Acknowledgments

We thank Dr Akira Kakizuka for kindly providing PGC-1α vector and helpful discussion. We also thank Dr Shunsuke Ishii for kindly providing Mybbp1a vector, Tamagawa Seiki Co. Ltd for providing tosyl-activated magnetic beads, Ms Ryoko Otsuki, Suzuyo Furukawa for technical assistance, Drs Eri Mukai and Yuichi Nishi for technical support and Drs Masahiko Sugita and Fuyuki Ishikawa for discussion. This work was supported by a Grant-in-Aid for Scientific Research from the Ministry of Education, Culture, Sports, Science, and Technology of Japan. This work was also supported in part by the Program for the Promotion of Fundamental Studies in Health Sciences of the National Institute of Biomedical Innovation (NIBIO). E.Y. was supported by a Research Fellowship from the Japan Society for the Promotion of Science for Young Scientists.

Author contributions

E.Y. designed and performed the experiments and wrote the manuscript with the help of S.F., N.I., J.Y. and H.M. E.Y., S.F., N.I and H.M. analysed the data. K.O. performed mass spectrometry analysis. S.M. prepared protein-immobilized beads. J.Y. directed the project as the principal investigator. H.M. supervised the study. All authors discussed the results and commented on the manuscript.

Additional information

Supplementary Information accompanies this paper on http://www.nature.com/naturecommunications

Competing financial interests: The authors declare no competing financial interests.

Reprints and permission information is available online at http://npg.nature.com/reprintsandpermissions/

How to cite this article: Yoshihara, E. *et al.* Disruption of TBP-2 ameliorates insulin sensitivity and secretion without affecting obesity. *Nat. Commun.* 1:127 doi: 10.1038/ncomms1127 (2010).

RESEARCH PAPER

Islets 2:4, 247-251; July/August 2010; © 2010 Landes Bioscience

FGF-21 enhances islet engraftment in mouse syngeneic islet transplantation model

Taeko Uonaga,[1] Kentaro Toyoda,[1] Teru Okitsu,[2] Xiaotong Zhuang,[1] Shunsuke Yamane,[1] Shinji Uemoto[3] and Nobuya Inagaki[1,4,*]

[1]Department of Diabetes and Clinical Nutrition; Graduate School of Medicine; Kyoto University; Sakyo-ku, Kyoto Japan; [2]Transplantation Unit; Kyoto University Hospital; Kyoto, Japan; [3]Department of Surgery; Division of Hepato-Pancreato-Biliary Surgery and Transplantation; Graduate School of Medicine; Kyoto University; Kyoto, Japan; [4]CREST of Japan Science and Technology (JST); Kyoto, Japan

Key words: fibroblast growth factor-21, diabetes mellitus, islet transplantation, β-cell load, insulin sensitivity, cytoprotection, apoptosis

Abbreviations: FGF-21, fibroblast growth factor-21; STZ, streptozotocin; FGFs, fibroblast growth factors; FGFRs, their corresponding receptors; s.c., subcutaneously; IPGTT, intraperitoneal glucose tolerance test; AUC, area under the curve; HE, hematoxylin-eosine; i.p., intraperitoneal injection; HBSS, hanks balanced salt solution; HEPES, 4-(2-hydroxyethyl)-1-piperazineethanesulfonic acid; RIA, radioimmunoassay

To clarify the effect of fibroblast growth factor-21 (FGF-21) on islet transplantation, a suboptimal number of islets were transplanted into streptozotocin (STZ)-induced diabetic mice with or without FGF-21 treatment. Three-day treatment with FGF-21 contributed to restoration of normoglycemia by suppressing islet graft loss. The FGF-21-treated mice showed lower glycemic levels despite similar insulin content in the graft than that in untreated mice on day 3, indicating that FGF-21 not only has a cytoprotective effect but also decreases β-cell load by increasing insulin sensitivity. These results suggest that FGF-21 may be useful as a treatment to improve islet engraftment rates in clinical islet transplantation.

Introduction

Fibroblast growth factors (FGFs) and their corresponding receptors (FGFRs) are known to be involved in the processes of development, transformation and angiogenesis.[1-4] The human FGF family consists of 22 members divided into seven subfamilies based on phylogeny and sequence identity.[1,5] On the other hand, FGFRs are divided into five distinct subtypes, FGFR-1 to -5, among which FGFR-1 and FGFR-2 are required for normal β-cell function and pancreatic development, respectively.[6-9] A co-factor usually is required for FGFs to bind and activate FGFR. Human FGF-21, which is mainly produced in liver, is a 181-amino-acid polypeptide and shares 75% amino acid sequence identity with mouse FGF-21.[10] FGF-21 together with FGF-19 and FGF-23 comprise the FGF-19 subfamily,[11] which is unique in that all three members are metabolic hormones involved in the regulation of glucose, lipid, bile acid and phosphate metabolism. FGF-21, the co-factor of which is βKlotho,[12,13] was first reported as a factor that might improve insulin sensitivity by upregulating glucose uptake into adipose tissue.[14] Subsequent studies showed that FGF-21 has various beneficial effects on pancreatic islets, increasing insulin synthesis and suppressing cytokine-induced apoptosis in isolated rat pancreatic islets and increasing glucose-induced insulin secretion from islets isolated from diabetic rodents.[15] Furthermore, FGF-21 reduces both plasma glucose and insulin levels not only in rodent diabetes models such as db/db mice but also in diabetic rhesus monkeys.[14-16]

Clinical islet transplantation has been performed world-wide since the report by Shapiro demonstrated 100% insulin independence in seven patients treated with a steroid-free, sirolimus-based immunosuppressant protocol, known as the Edmonton protocol.[17] However, one of the problems of this protocol is that multiple donors are required for insulin independence, mainly because of graft-loss caused by various stressors immediately after transplantation.[18,19] It is therefore especially important to reduce β-cell loss during this critical period.[20]

Because FGF-21 has various beneficial effects on islets, we investigated its effects on islet engraftment using syngeneic islet transplantation in diabetic mice with or without its administration during the critical 3 days after islet transplantation.

Results

FGF-21 ameliorated hyperglycemia in STZ-induced diabetic mice transplanted with a suboptimal number of islets. Eighty freshly isolated islets, which is a suboptimal number of islets for ameliorating hyperglycemia when transplanted alone, were transplanted into the left sub-renal capsule of STZ-induced diabetic mice. Immediately after transplantation, FGF-21 administration was begun subcutaneously (s.c.) twice daily for 3 days

*Correspondence to: Nobuya Inagaki; Email: inagaki@metab.kuhp.kyoto-u.ac.jp
Submitted: 03/01/10; Revised: 05/11/10; Accepted: 05/13/10
Previously published online: www.landesbioscience.com/journals/islets/article/12402

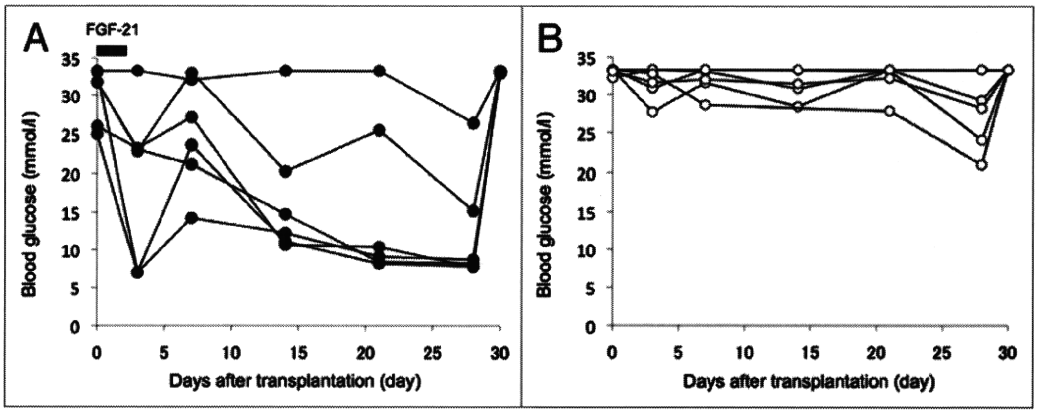

Figure 1. Non-fasting blood glucose levels in IT(+)/FGF(+) (closed circle, n = 6) (A) and IT(+)/FGF(-) mice (open circle, n = 5) (B).

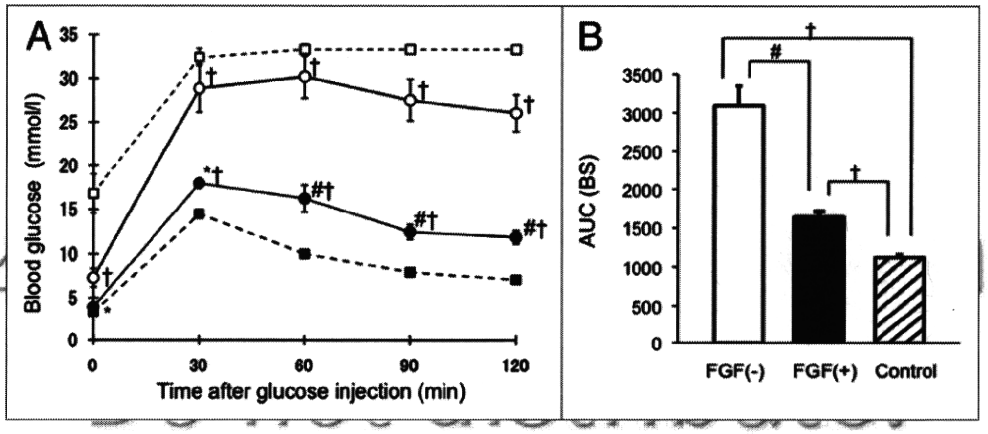

Figure 2. (A) Plasma glucose levels during i.p. glucose tolerance test (IPGTT) performed on day 30 in sham-operated wild-type C57BL/6 mice (control, dotted line, closed square, n = 5), in normoglycemic IT(+)/FGF(+) mice with non-fasting blood glucose level below 11.1 mM (closed circle, n = 4), in IT(+)/FGF(-) mice (open circle, n = 5), and in STZ-induced diabetic mice (dotted line, open square, n = 3). (B) AUC of blood glucose levels during IPGTT in wild-type control (lined bar), IT(+)/FGF(+) (black bar), and IT(+)/FGF(-) mice (white bar). *p < 0.05 vs. IT(+)/FGF(-). #p < 0.01 vs. IT(+)/FGF(-), †p < 0.01 vs. control.

(from day 0 through day 2). As control, 80 freshly isolated islets were similarly transplanted to STZ-induced diabetic mice but without FGF-21 treatment. As in our previous report, the criterion of normoglycemia was defined as a non-fasting blood glucose level below 11.1 mM (200 mg/dl) on at least two consecutive measurements on different day time points.[21]

After islet transplantation, 66.7% of the mice treated with FGF-21 (IT(+)/FGF(+) mice) became normoglycemic (**Fig. 1A**), while all of mice without FGF-21 treatment (IT(+)/FGF(-) mice) remained hyperglycemic (**Fig. 1B**). Mean blood glucose levels were significantly lower in IT(+)/FGF(+) mice than those in IT(+)/FGF(-) mice on day 3, and the difference continued thereafter (Day 0: 30.2 ± 1.5 vs. 33.1 ± 0.2 ($p = 0.11$), Day 3: 19.4 ± 4.3 vs. 31.6 ± 1.1 ($p < 0.05$), Day 7: 25.2 ± 2.9 vs. 32.0 ± 0.9 ($p = 0.07$), Day 14: 17.1 ± 3.6 vs. 31.4 ± 1.2 ($p < 0.05$), Day 21: 15.8 ± 4.4 vs. 32.2 ± 1.1 ($p < 0.01$), Day 28: 12.4 ± 3.0 vs. 28.2 ± 2.5 ($p < 0.01$) (mM)). The removal of the left kidney bearing the islet grafts resulted in hyperglycemia in all recipient mice (**Fig. 1**). Sham-operated STZ-induced diabetic mice with and without FGF-21 treatment showed persistent hyperglycemia (data not shown). These results indicate that FGF-21 improved glycemic control in islet-transplanted STZ-induced diabetic mice. Mean body weight on day 7 in IT(+)/FGF(+) mice was significantly lower than that in IT(+)/FGF(-) mice (20.3 g vs. 21.8 g, $p < 0.05$), but body weight on day 28 was similar in both of these mice (23.6 g vs. 23.1 g, $p = 0.35$).

FGF-21 treatment improved glucose tolerance 30 days after islet transplantation. To evaluate the degree of glucose tolerance, we performed intraperitoneal glucose tolerance test (IPGTT) on day 30 in hyperglycemic IT(+)/FGF(-) mice and normoglycemic IT(+)/FGF(+) mice (**Fig. 2A and B**). Blood glucose levels and area under the curve (AUC) during IPGTT in normoglycemic IT(+)/FGF(+) mice were significantly lower than those in hyperglycemic IT(+)/FGF(-) mice. However, both the blood glucose concentration and AUC in normoglycemic IT(+)/FGF(+) mice were not improved to the level observed in wild-type mice.

Islet grafts were more preserved in FGF-21-treated mice than those in untreated mice on day 30. To determine islet mass, we performed Hematoxylin-Eosine (HE) staining and insulin-immunostaining. Islet grafts in normoglycemic IT(+)/FGF(+) mice and those in hyperglycemic IT(+)/FGF(-) mice were detectable and comparable on day 3 (**Fig. 3A, B, E and**

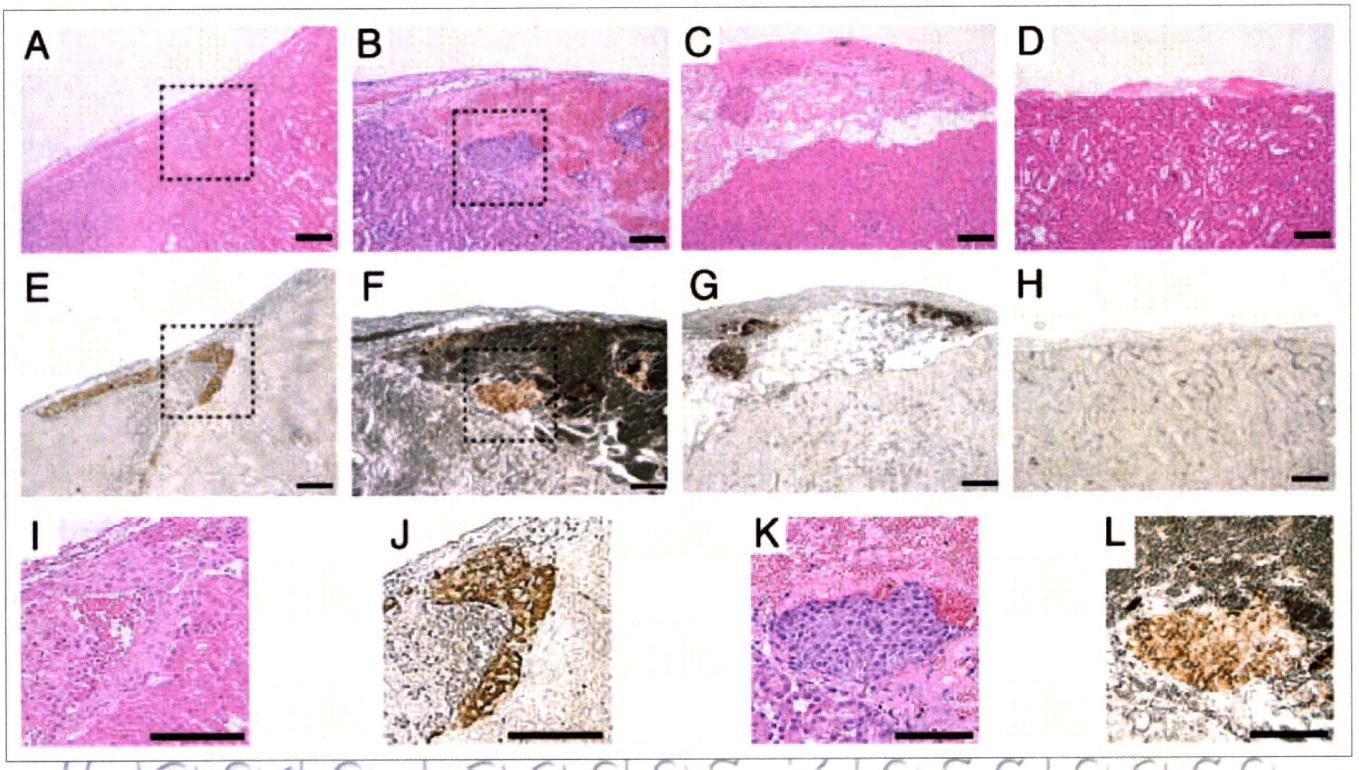

Figure 3. Immunohistochemical analysis of islet grafts from IT(+)/FGF(+) (A, C, E and G) and IT(+)/FGF(-) (B, D, F and H) mice. HE staining (x200) (A–D) and insulin-immunostaining (x200) (E–H) were performed. Ensquared areas in (A, B, E and F) are magnified in (I,K,J and L) respectively. Bar = 100 μm.

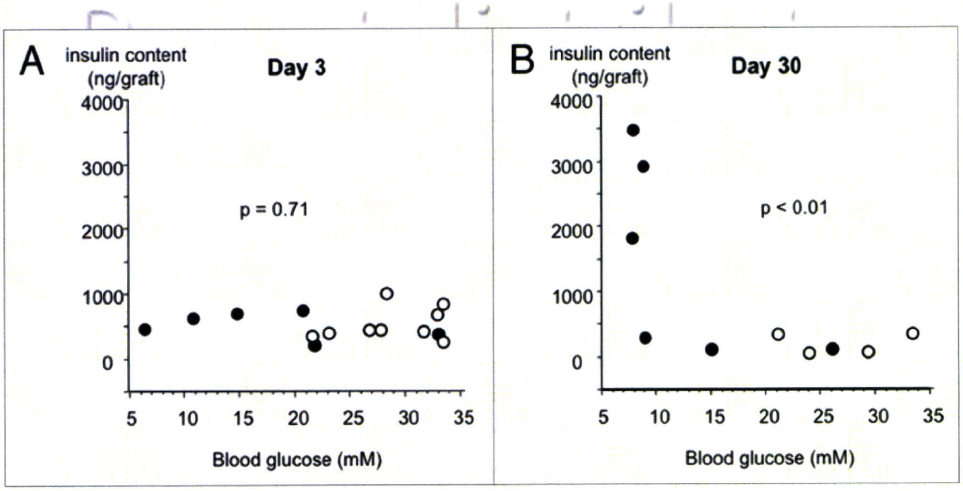

Figure 4. Insulin contents of islet grafts were measured in both IT(+)/FGF(+) (closed circle) and IT(+)/FGF(-) mice (open circle) on day 3 (A) and day 30 (B). Insulin contents of islet grafts were not correlated with the levels of blood glucose on day 3 ($p = 0.71$) (A), but were inversely correlated on day 30 ($p < 0.01$) (B).

F). Insulin content on day 3 in both mice was similar (**Fig. 4A**). However, on day 30, islet grafts in normoglycemic IT(+)/FGF(+) mice were more readily detectable (**Fig. 3C and G**), while those in IT(+)/FGF(-) mice were barely detectable (**Fig. 3D and H**). Consistently with this immunohistochemical finding, insulin content on day 30 in normoglycemic IT(+)/FGF(+) mice was significantly greater than that in untreated mice [2117.8 vs. 199.5 (ng/graft), $p < 0.05$] (**Fig. 4B**). We then analyzed the relationship between insulin content in the grafts and the non-fasting blood glucose level in all of the mice in both groups. Spearman rank correlation assessment showed that insulin content was inversely correlated with the non-fasting blood glucose level on day 30 ($p < 0.05$) (**Fig. 4B**), while no correlation was observed on day 3 ($p = 0.71$) (**Fig. 4A**).